

THE CONNECTION BETWEEN GALAXIES AND DARK MATTER STRUCTURES IN THE LOCAL UNIVERSE

RACHEL M. REDDICK^{1,2}, RISA H. WECHSLER^{1,2}, JEREMY L. TINKER³, AND PETER S. BEHROOZI^{1,2}
¹ Kavli Institute for Particle Astrophysics and Cosmology, Physics Department, Stanford University, Stanford, CA 94305, USA;
rredd@stanford.edu, rwechsler@stanford.edu

² SLAC National Accelerator Laboratory, Menlo Park, CA 94025, USA

³ Physics Department, New York University, New York, NY 10003, USA

Received 2012 July 6; accepted 2013 May 16; published 2013 June 12

ABSTRACT

We provide new constraints on the connection between galaxies in the local universe, identified by the Sloan Digital Sky Survey, and dark matter halos and their constituent substructures in the Λ -cold dark matter model using WMAP7 cosmological parameters. Predictions for the abundance and clustering properties of dark matter halos, and the relationship between dark matter hosts and substructures, are based on a high-resolution cosmological simulation, the Bolshoi simulation. We associate galaxies with dark matter halos and subhalos using subhalo abundance matching, and perform a comprehensive analysis which investigates the underlying assumptions of this technique including (1) which halo property is most closely associated with galaxy stellar masses and luminosities, (2) how much scatter is in this relationship, and (3) how much subhalos can be stripped before their galaxies are destroyed. The models are jointly constrained by new measurements of the projected two-point galaxy clustering and the observed conditional stellar mass function of galaxies in groups. We find that an abundance matching model that associates galaxies with the peak circular velocity of their halos is in good agreement with the data, when scatter of 0.20 ± 0.03 dex in stellar mass at a given peak velocity is included. This confirms the theoretical expectation that the stellar mass of galaxies is tightly correlated with the potential wells of their dark matter halos before they are impacted by larger structures. The data put tight constraints on the satellite fraction of galaxies as a function of galaxy stellar mass and on the scatter between halo and galaxy properties, and rule out several alternative abundance matching models that have been considered. This will yield important constraints for galaxy formation models, and also provides encouraging indications that the galaxy–halo connection can be modeled with sufficient fidelity for future precision studies of the dark universe.

Key words: dark matter – galaxies: formation – galaxies: groups: general – galaxies: halos – large-scale structure of universe – methods: statistical

Online-only material: color figures

1. INTRODUCTION

The connection between galaxies and their dark matter halos is the fundamental link between predictions of a given cosmological model and models of galaxy formation. Galaxies form in the gravitational potential wells of dark matter halos, and our modern understanding of galaxy formation therefore depends on an understanding of dark matter. Dark matter halos are virialized structures that began as high-density peaks in the early universe and grew and collapsed through self-gravity. Halos grow by accreting additional material from the smooth density field as well as nearby smaller halos. The galaxies within them grow in tandem with their respective halos. Accreted halos (or subhalos) generally also contain galaxies. These subhalos (and the galaxies they contain) are stripped by the tidal forces of the (host) halo that have accreted them and are eventually destroyed. The halo that accreted the subhalo gains this mass, and the stellar mass of the disrupted galaxy either accretes onto another galaxy in the host halo or is dispersed into the intracluster light.

Given this general understanding of the relationship between galaxies and dark matter, it is possible to predict the spatial distribution of galaxies from an N -body simulation of dark matter only. The baryonic matter of the galaxies is a small fraction of all matter, and its effects on the formation of dark matter halos are subdominant, with observable impacts

only on small scales (Kravtsov et al. 2004; Springel et al. 2005; Trujillo-Gomez et al. 2011). However, populating a dark matter simulation with galaxies requires a detailed model to connect the dark matter with the galaxies. Precise models of this galaxy–halo connection and its evolution are important for constraining galaxy formation models. They are also of increasing importance in the era of precision cosmology. In particular, the detailed relationship between the dark matter distribution—directly related to cosmological parameters—and the galaxies that trace it is likely to be a dominant systematic in studies of cosmic acceleration with galaxy surveys using a range of probes (e.g., Cacciato et al. 2009; More et al. 2009; Tinker et al. 2011; Nuza et al. 2013, and references therein).

The most direct approach to understanding the relationship between galaxies and halos is to run a full, hydrodynamic simulation, which may explicitly include the effects of star formation and feedback (e.g., Bryan & Norman 1998; Springel & Hernquist 2003; Vogelsberger et al. 2012, and references therein). Unfortunately, this approach remains computationally expensive, and therefore cannot currently be applied to large volumes. Additionally, the results are complicated by differences in numerical techniques and the treatment of important physics below the resolution limit of the simulation. An alternative is to use a semi-analytical model of galaxy formation (see, e.g., Somerville et al. 2012; Lu et al. 2012; Henriques et al. 2012; Benson 2012 for recent examples). This has the advantage of

including many different processes that act on the galaxies in question, such as relations between star formation and feedback. However, these models tend to be complex, having many parameters and requiring careful tuning, complicating efforts to understand the underlying physics. A simpler option is to use a halo occupancy distribution (HOD), which is based on knowing the number of galaxies of some type that may be assigned to each halo (e.g., Yang et al. 2008, 2009; Zehavi et al. 2011; Leauthaud et al. 2012, and references therein). This approach still has the difficulty of using many parameters, and therefore requires multiple measurements of the galaxy distribution as inputs to constrain the model.

An alternative to these is a semi-empirical approach known as subhalo abundance matching (Kravtsov et al. 2004; Vale & Ostriker 2004). Rather than input galaxy formation processes directly, abundance matching models make the simple assumption that some halo property is monotonically related to some galaxy property, typically galaxy luminosity or stellar mass. That is, each halo (or subhalo) contains one galaxy at its center, whose luminosity or stellar mass is determined by some property of its host. This property is often related to the host halo mass, but there are many different possibilities. Additional choices must be made to specify the specific model, such as whether to include nonzero scatter between the given halo property and the galaxy stellar mass. Nonetheless, abundance matching models have the advantage of requiring few (or no) parameters, and using the full predictions of numerical simulations to model the dark matter distribution into the fully nonlinear regime.

In general, for a given input luminosity or stellar mass function (SMF), abundance matching can produce a galaxy population that accurately reproduces measured galaxy statistics and provides insight into galaxy formation (Conroy et al. 2006; Vale & Ostriker 2006; Moster et al. 2010; Behroozi et al. 2010). Previous studies have demonstrated that abundance matching models are generally sufficient to statistically reproduce the observable properties of galaxies, including the two-point clustering, the galaxy bias, and the Tully–Fisher relation (Vale & Ostriker 2004; Conroy et al. 2006; Trujillo-Gomez et al. 2011). Recent improvements in numerical dark matter simulations present the opportunity to test this model on a simulation large enough to have excellent statistics for L^* galaxies while resolving halos small enough to host galaxies as dim as the Magellanic Clouds. Bolshoi is one such simulation, which also uses cosmological parameters consistent with WMAP5 and other measurements (Klypin et al. 2011). Trujillo-Gomez et al. (2011) showed that an abundance matching model applied to halos in this simulation could provide a good match to clustering statistics and the Tully–Fisher relation.

Testing any model requires statistics of the galaxy distribution. The Sloan Digital Sky Survey (SDSS; Abazajian et al. 2009) has provided a quantitative advance in measuring galaxy statistics in the local universe, yielding increasingly precise measurements of the clustering of galaxies (e.g., Zehavi et al. 2011) and large numbers of groups or clusters (e.g., Koester et al. 2007; Yang et al. 2007). Because measurements of cosmological parameters depend heavily on galaxies as tracers, the systematics of such measures may be reduced by an improved understanding of how galaxies are associated with dark matter (e.g., Rozo et al. 2010; Tinker et al. 2012; More et al. 2012).

Our intent is two-fold: (1) to examine the ability of different abundance matching models to simultaneously reproduce the correlation function and conditional stellar mass function

(CSMF) measured from the SDSS, and (2) to systematically test the underlying assumptions in the abundance matching ansatz. To do so, we also make new measurements of the clustering and conditional stellar mass functions from the SDSS.

We first describe the data used in our study (Section 2). This is followed by a description of the Bolshoi simulation and the models considered (Section 3). Section 4 describes our measurements of the correlation function and the CSMF, and additional statistics of the galaxies in groups. An evaluation of how these vary as the model parameters are varied is presented in Section 5. The principle results of this work are the constraints on the model parameter space derived from these measurements (Section 6). We then consider the impact of using different SMFs and a comparison with another measurement of the CSMF (Section 7). A summary of our results and conclusions may be found in Section 8. We find that our best-fit model provides an excellent fit to the data. We also find that the parameters in the model are well constrained, and that models that abundance match to many commonly used halo properties are ruled out by current data.

Throughout this work, we assume the same cosmology as the Bolshoi simulation, using Λ -cold dark matter (Λ CDM) with $\Omega_m = 0.27$, $\Omega_\Lambda = 1 - \Omega_m$, $\Omega_b = 0.042$, $\sigma_8 = 0.82$, and $n = 0.9$. Absolute magnitudes and stellar masses are quoted with $h = 1$. Except where otherwise specified, stellar masses are those given by the KCORRECT algorithm of Blanton & Roweis (2007). We use \log for the base-10 logarithm, and \ln for the natural logarithm. Halo masses are given in terms of the virial mass, here defined as the mass within a radius such that the average enclosed density is $\Delta_{\text{vir}}\rho_{\text{crit}}\Omega_m$ for $\Delta_{\text{vir}} = 360$ at $z = 0$ as given by Bryan & Norman (1998) unless stated otherwise.

When referring to dark matter halos, the terms “halo” or “host halo” are used to refer to distinct halos only, which do not lie within the virial radius of a more massive dark matter halo. In contrast, “subhalo” is used to refer to dark matter halos whose centers lie within the virial radius of a more massive halo. A galaxy group is a set of galaxies that all lie within the virial radius of the same (distinct) halo, which may range in size from only one galaxy up to galaxy clusters. A central galaxy (or “central”) is the galaxy which resides at the center of a halo. Satellite galaxies (or just “satellites”) are those which reside in subhalos inside a more massive dark matter halo.

2. SDSS DR7 DATA

Our study uses the New York University Value Added Galaxy Catalog (NYU-VAGC; Blanton et al. 2005), based on Data Release 7 of the SDSS (Padmanabhan et al. 2008; Abazajian et al. 2009). We focus primarily on two measurements: the projected two-point correlation function and the CSMF. To measure the clustering, we use a set of volume-limited samples corresponding to a series of cuts in stellar mass. For the group statistics such as the CSMF, we focus on one volume-limited sample, with a cut in absolute r -band luminosity of $M_r - 5 \log h < -19$. The area of the sample we use is 7235 deg^2 , with a median redshift of $z = 0.05$. The $M_r - 5 \log h < -19$ sample contains a total of 74,987 galaxies with a maximum redshift of $z = 0.064$, covering a volume of roughly $4.8 \times 10^6 (h^{-1} \text{ Mpc})^3$. We focus on the distribution of galaxies in terms of their stellar mass. Throughout, we quote stellar masses in $M_\odot h^{-2}$. The cut of $\log(M_*) > 9.8$ leaves a complete sample of 54,119 galaxies in the same range in redshift.

The details of the group finder are described in the appendix of Tinker et al. (2011), which is based on the algorithm of

Yang et al. (2005). Galaxy groups are found by initially doing “inverse” abundance matching. The highest host halo mass expected in the observed volume is assigned to the most massive galaxy. The next most massive galaxy that is not within the virial radius of the most massive halo is assigned the second most massive host halo, and so on. This matching is done with zero scatter, using the mass function of Tinker et al. (2008). Galaxies within the virial radii of the assigned host halos are treated as satellites. This initial assignment is used to calculate an initial group stellar mass for each group. Groups are then reassigned host halo masses using the total stellar mass within the virial radius of the initially assigned halos. This procedure is iterated until group assignments remain unchanged. These results are distinct from the results of Tinker et al. (2011) in that we use $\Delta_{\text{vir}} = 360$, rather than 200, for consistency with the mock catalogs, and in how the initial halo-to-galaxy assignment is done. This results in a total of $\sim 43,000$ groups, of which 17,178 are assigned a host halo mass greater than $10^{12} M_{\odot}$. We impose this limit because below a mass of $\sim 10^{12} M_{\odot}$ essentially all “groups” have only one galaxy above the $\log(M_{*}) > 9.8$ threshold. Therefore, the group assignment is not very informative below this mass.

The group finder introduces two major sources of bias. First, groups with low total stellar mass may consist of only one or two galaxies. Because host masses are assigned based on total group stellar mass, the assigned host halo mass relates directly to the stellar mass of the dominant galaxy. This artificially reduces the scatter between the central galaxy stellar mass and the host halo mass for low-mass host halos. Second, the assumption that the galaxy with the most stellar mass is the central is not always true (e.g., Skibba et al. 2011) and can bias results based on the central galaxies. To take these changes into account, we create a galaxy distribution by populating halos in the simulation, and this galaxy distribution is passed through the group finder before making comparisons to the groups found in the volume-limited catalog. The effects of group finding on our measurements are discussed in more detail in Section 7.3 and Appendix A.

The NYU-VAGC is based on the SDSS spectroscopic sample. This allows precision measurements of redshifts, which are required for measuring the projected two-point correlation function and to making group assignments. However, the spectroscopy was obtained by assigning targets to spectroscopic plates connected to a fiber-fed spectrograph. The size of the fibers prevents any two targets separated by $55''$ or less from being observed at the same time on the same plate. Though overlapping plates partially alleviates this problem, a significant fraction of galaxies in the sample lack redshifts for this reason. These galaxies are “fiber collided”; this occurs for $\sim 5\%$ of the galaxies in our sample. A detailed explanation of the SDSS survey and hardware can be found in Stoughton et al. (2002). The tiling algorithm for the spectroscopic plates is described in Blanton et al. (2003b).

Our clustering measurements were made on the same volume-limited sample as the groups. Clustering measurements are presented in Section 5, with the error estimation discussed in Section 4.

To use the fiber-collided galaxies, the simplest correction is to assign the galaxy the redshift of the galaxy with which it is fiber collided. As demonstrated by Zehavi et al. (2005), this correction is adequate for the correlation function down to scales of $\sim 0.1 \text{ Mpc h}^{-1}$. However, it has a significant impact on the CSMF, since a fiber-collided galaxy is likely to be assigned to the same group as the galaxy it is fiber collided with. Our volume-

limited sample has a median redshift of $z = 0.05$. At this redshift, the $55''$ angle corresponds to $\sim 40 \text{ kpc h}^{-1}$ (comoving).

3. SIMULATED GALAXY CATALOGS

3.1. Simulations

The Bolshoi simulation is a recently completed cosmological dark matter simulation, described in Klypin et al. (2011). The simulation uses 2048^3 particles and has a volume of $(250 \text{ Mpc h}^{-1})^3$, roughly three times bigger than the SDSS $M_r < -19$ volume-limited sample. The large volume is combined with the capability to resolve subhalos, dark matter halos that lie within the virial radius of larger host halos, down to a circular velocity of $\sim 55 \text{ km s}^{-1}$. This permits a precise study of subhalos and the satellite galaxies that inhabit them.

Because our models rely on abundance matching, we require knowledge of the dark matter halo distribution. Therefore, halo finding is necessary to locate the potential wells where galaxies form. There are several different algorithms used for this purpose, and they may produce different results even when working on the same test halos (see Knebe et al. 2011; Onions et al. 2012, and references therein). For our work, we use the ROCKSTAR halo finder (Behroozi et al. 2013b), which has the advantage of using velocity as well as position information to locate substructure. This halo finder produces results that are comparable to other modern halo finders (e.g., bound density maxima (BDM) and Amiga’s Halo Finder) on small scales; the use of phase space information allows it to track subhalos better in the inner regions of their hosts (Knebe et al. 2011; Onions et al. 2012; Behroozi et al. 2013b). The halo (and subhalo) masses and maximum circular velocities (v_{max}) are calculated using only bound particles, but including substructures. We also use the merger trees produced by the algorithm described in Behroozi et al. (2013c). The merger trees allow us to use the past history of the halos and subhalos when assigning galaxy properties. This combination of codes provides better tracking of subhalos over time (Behroozi et al. 2013c).

3.2. Abundance Matching

Abundance matching is a simple and effective method for associating dark matter halos with galaxies (see, e.g., Kravtsov et al. 2004; Vale & Ostriker 2004; Conroy et al. 2006; Behroozi et al. 2010; Moster et al. 2010). A simple example is that given halo mass and SMFs, halos are assigned galaxies so that the most massive halo hosts the most massive galaxy, the second most massive halo hosts the second most massive galaxy, and so on. More generally, this approach is complicated by scatter in the halo-mass–stellar-mass relation (e.g., Tasitsiomi et al. 2004; Behroozi et al. 2010), and the question of which halo property is more closely correlated with galaxy stellar mass (Conroy et al. 2006). We consider both the effect of various nonzero values of scatter and the use of different halo properties on observable galaxy properties.

The most natural theoretical expectation may be that galaxy properties are strongly correlated with the depth of their potential wells. If this is the case, the property v_{max} is likely to be the most relevant for galaxy properties. Dark matter halos can be significantly stripped after they are influenced by larger halos (before or after they enter the virial radius), in a way that galaxies are not. Because of this, it is reasonable to expect that galaxy properties should be most strongly correlated with their mass before this stripping occurs (see, e.g., discussion in Conroy et al. 2006). At present, there is still a wide range of halo

properties used in the literature. For completeness, we consider a range of possible choices for the halo properties, and evaluate their consistency with data.

1. M_0 . This is the simplest form of abundance matching, using only the masses of halos (or subhalos) at the present time. Note that the mass of a subhalo is not measured out to the subhalo's virial radius; the subhalos identified by ROCKSTAR include all particles that are bound to the subhalo (see Behroozi et al. 2013b for further details). Because the subhalos' dark matter is more readily stripped than the galaxies hosted at their centers, the M_0 approach generally underestimates satellite stellar masses (or luminosities) (Behroozi et al. 2013a).
2. M_{acc} : the mass of halos at accretion, or infall. For (distinct) halos, this is the mass at the present time, the same as M_0 . For subhalos, this is the mass of the halo when it crosses the virial radius of its host, and is generally greater than M_0 . This boosts the stellar mass of satellites relative to centrals of the same M_0 .
3. M_{peak} : the maximum mass that the halo (or subhalo) has ever had in its merger history. This mass is nearly the same as M_0 for isolated halos, but may be significantly greater for subhalos than either their present mass or their mass at infall, as some fraction of halos will be stripped prior to accretion. Behroozi et al. (2013a) have found that most subhalos start being stripped at $\sim 3 R_{\text{vir}}$, regardless of host mass.
4. $M_{0,\text{peak}}$. For isolated halos, this is equal to M_0 ; for subhalos, it is equal to M_{peak} .
5. v_{max} . Similar to M_0 , v_{max} is the maximum circular velocity of a halo (or subhalo) at the present time. This model generally suffers from the same difficulties as M_0 , having too few satellite galaxies with a given stellar mass.
6. v_{acc} . As with M_{acc} , v_{acc} is the maximum circular velocity of a halo at the present time (equivalent to v_{max} for isolated galaxies), or at the time of infall. As with M_0 , this boosts the stellar mass of satellites over that when using v_{max} , increasing the satellite fraction at a given stellar mass.
7. v_{peak} . Similar to M_{peak} , v_{peak} is the highest circular velocity a halo has had over its entire merger history. This is generally slightly greater than v_{max} or v_{acc} for isolated halos and significantly greater than either v_{max} or v_{acc} for subhalos.
8. $v_{0,\text{peak}}$. Similar to $M_{0,\text{peak}}$, $v_{0,\text{peak}}$ assigns the halos their present maximum circular velocity, and the subhalos their peak circular velocity. Because $v_{0,\text{peak}}$ has the largest difference between (distinct) halos and subhalos, this is the model with the most massive satellite galaxies, and consequently the highest satellite fractions.

A comparison of how the properties we discuss here change for a single halo can be seen in Figure 1.

Additionally, there is a significant difference between the v_{max} - and M_0 -based matching. In particular, a direct comparison between v_{peak} and M_{peak} shows that at fixed M_{peak} , subhalos tend to have slightly higher peak v_{max} (by as much as $\sim 7\%$; see Figure 2). This may be due to a combination of two factors. One is that less concentrated subhalos may be more easily disrupted, and less likely to survive to be included in the sample. An alternative is halo assembly bias (e.g., Wechsler 2001; Gao & White 2007; Wechsler et al. 2006). In this case, smaller halos that formed earlier and in lower-density regions, prior to accretion, tend to have higher concentrations. This alternative is plausible, as it has been demonstrated in Guo et al. (2011)

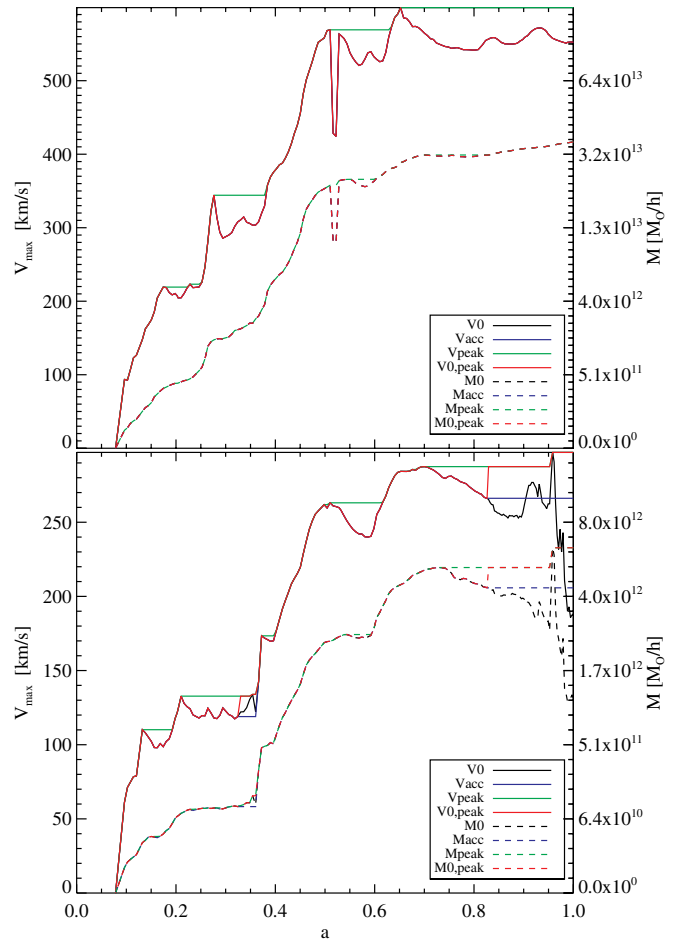


Figure 1. Top: evolution of various halo properties with scalefactor a , for a single central galaxy, whose host halo has a mass of 3.7×10^{13} at $z = 0$. Note that the distinct halo has no mass loss, so $M_0 = M_{\text{acc}} = M_{\text{peak}} = M_{0,\text{peak}}$. Further, $v_{\text{max}} = v_{\text{acc}} = v_{0,\text{peak}}$ by definition. Only when v_{max} drops significantly following a merger (due to the drop in concentration) does v_{peak} deviate from v_{max} . Bottom: the same plot, but for a galaxy which is a satellite at $z = 0$, with a present mass of 1.2×10^{12} in a host of mass 3.1×10^{13} . The satellite is accreted at around $a = 0.85$. Prior to this time, it is a central halo with the same general properties as in the top plot. After accretion, however, v_{acc} is fixed, and $v_{0,\text{peak}} = v_{\text{peak}}$. Because the halo starts being stripped here as well, M_0 is no longer the same as the other mass measures; the rest, however, remain identical. The jumps at $a = 0.95$ are associated with a merger event between this particular subhalo and another subhalo.

(A color version of this figure is available in the online journal.)

and Rodríguez-Puebla et al. (2012) that satellite galaxies tend to have slightly more stellar mass than central galaxies with the same (sub)halo mass. This difference is most significant in less massive host halos. A test using a lower-resolution simulation (the Consuelo simulation discussed in Appendix B) recovers the same difference in v_{peak} between halos and subhalos, suggesting that this difference is not likely due to resolution issues.

The impact of changing the abundance matching parameter is discussed in Section 5.1. Conroy et al. (2006) considered the use of v_{max} and v_{acc} , concluding that v_{acc} was able to reproduce the two-point correlation function, but v_{max} was not. Most related studies have used one of these two properties.

To perform abundance matching, we use the SMF of the relevant galaxy sample as input. Because the conditional mass and luminosity functions are sensitive to this input, for consistency with the group catalog, we use the exact SMF of galaxies in the corresponding volume-limited sample to perform the abundance

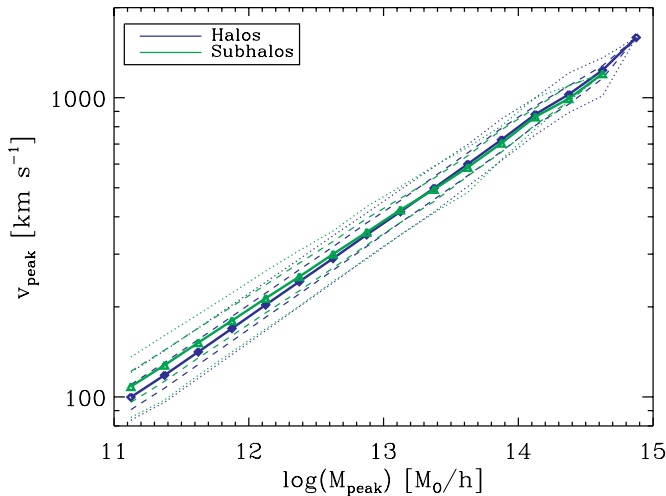


Figure 2. Relationship between v_{peak} and M_{peak} for satellites and central galaxies. The solid blue line indicates the median v_{peak} at fixed M_{peak} for distinct halos. The dashed and dotted lines indicate the 68% and 95% bounds, respectively. The green lines are the corresponding results for subhalos. Note that subhalos tend to have larger v_{peak} and a wider dispersion, particularly at low masses, where the difference in the medians is $\sim 10\%$.

(A color version of this figure is available in the online journal.)

matching instead of using the global relations in the literature (e.g., Li & White 2009; Yang et al. 2009; Baldry et al. 2012).

Scatter is introduced using the deconvolution method described in Behroozi et al. (2010). In brief, first abundance matching with zero scatter ($\sigma = 0$) is performed using the observed SMF. A log-normal scatter is added to the stellar masses of the galaxies. The “intrinsic” SMF, that is, the SMF to which scatter is added in order to produce the observed SMF, is estimated based on the difference between the observed and scattered SMFs. This new “intrinsic” SMF is then used in abundance matching. This procedure is repeated until the output of the step where scatter is added is sufficiently close to the observed SMF. While generally accurate, this approach is incapable of adding extremely high scatter and maintaining the steepness of the SMF above the characteristic stellar mass $M_{*,s}$ (see Figure 3). This is not a significant problem, as such large scatter (above ~ 0.3 dex at fixed stellar mass) appears to be excluded by data at least for galaxies more massive than $M_{*,s}$. This has been shown by previous authors (More et al. 2009; Leauthaud et al. 2012), and is shown to be excluded by our later analysis. An alternative method of introducing scatter, presented in Trujillo-Gomez et al. (2011), avoids this problem by selecting stellar masses from a predetermined list, guaranteeing that the SMF is exactly reproduced. This method does not assume constant log-normal scatter in stellar mass, and therefore yields a somewhat skewed distribution of galaxy stellar masses in large dark matter halos compared to a log-normal. It is not yet clear whether these alternatives can be distinguished by existing data.

In applying this model, we do not include any impact from statistical errors in the stellar mass measurements. Therefore, the scatter we measure will be a combination of scatter in observed stellar masses and in stellar mass at fixed host halo mass.

In addition to the scatter, we consider the possibility that satellite galaxies are disrupted before their halos are destroyed in the simulation. To investigate this possibility, we introduce a cutoff on the mass of subhalos. Once a subhalo falls below some fraction of its maximum past mass M_{peak} , we consider its galaxy to have been disrupted, similar to the cutoff examined in Wetzel

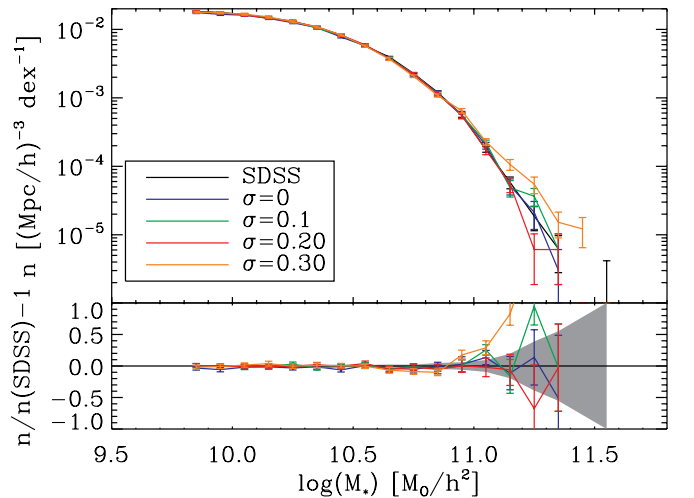


Figure 3. Stellar mass function (SMF) from the SDSS sample (black), used as input to the abundance matching, compared against the output results of abundance matching and observational systematics (colored lines: blue, green, red, and orange correspond to 0, 0.1, 0.2, and 0.3 dex of scatter). Note that high values of scatter force the bright end of the stellar mass function high because this steep region cannot be produced by convolution with a too-broad Gaussian. Because there is no dependence of the scatter on the matching parameter used or μ_{cut} , there is little change in the SMF between models at fixed scatter. Error bars are derived from jackknife resampling.

(A color version of this figure is available in the online journal.)

& White (2010). These disrupted subhalos are excluded from abundance matching. Effectively, we assign disrupted subhalo galaxies with zero stellar mass. We use the parameter μ_{cut} to define the cutoff fraction of M_{peak} , ignoring all (sub)halos for which $M_0 < \mu_{\text{cut}} M_{\text{peak}}$. We consider a range of μ_{cut} from 0 (all subhalos are assigned a galaxy) to 0.15. For reference, a value of $\mu_{\text{cut}} = 0.1$ removes $\sim 4\%$ of subhalos that would have been included in the sample with $\mu_{\text{cut}} = 0$.

Once the abundance matching has been performed, we convert the Bolshoi snapshot into a lightcone by taking the origin as the point of observation. This allows us to produce an octant on the sky, including redshifts, to a depth of $z = 0.083$. We use the snapshot at the mean redshift of the data, $z = 0.05$, and ignore evolution in the dark matter distribution over this narrow range. To introduce the same systematics present in the group catalog, we first add fiber collisions (as described below), then use the group finder to find galaxy groups and determine whether galaxies are centrals or satellites.

3.3. Simulated Fiber Collisions

Once the mock catalog has been converted into a lightcone, it is necessary to consider the effect of fiber collisions. Fiber collisions must be determined prior to using the group finder.

We use the Bolshoi simulation to provide the volume-limited sample. The sample of interest extends to a redshift of 0.063. We use the remaining volume of Bolshoi, to a redshift of 0.083, to provide a background of galaxies that may be collided. Following this procedure, we find $\sim 4\%$ of galaxies are fiber collided for the volume-limited sample with $\log(M_*) > 9.8$, compared to $\sim 5\%$ of galaxies in our sample. The algorithm that is applied to the SDSS for determining the locations of spectroscopic fibers is discussed in Blanton et al. (2003b). We use a related algorithm applied to the mock lightcones. We initially include galaxies above the stellar mass limit at any given redshift. Galaxies that have neighbors within $55''$ are then placed into “collision groups” of nearby galaxies. Of these galaxies, one

is chosen to be the galaxy for which a true redshift is known. Some of the other galaxies may also have “measured” redshifts, partly at random and partly depending on the geometry of the collision group. The remainder are considered fiber collided with the nearest galaxy on the sky, and assigned its redshift.

After the mock catalogs are completed, we then apply the same group finder as used on the SDSS groups to the mock catalogs. This allows us to select galaxy groups consistently.

4. MEASUREMENTS

We use multiple measurements on both the SDSS DR7 catalog and the synthetic galaxy catalogs constructed by populating simulations with abundance-matched galaxies. In particular, we focus on the projected two-point correlation function and the CSMF, and use these in constraining our models. We also consider other measurements, such as the group stellar mass function (GSMF) and the satellite fraction, to provide additional tests and to better understand the underlying galaxy distribution.

4.1. Projected Correlation Function

In its most basic form, the two-point correlation function counts pairs of galaxies at different separations, relative to the number of such pairs one would expect from a random distribution (see, e.g., Davis et al. 1985; Zehavi et al. 2005). A clustered distribution, such as occurs in dark matter halos and thus, in galaxies, results in a larger value for the correlation function. Smaller scales ($< \sim 1$ Mpc h^{-1}) generally correspond to clustering in a single host halo, between the central galaxies and its satellites and between pairs of satellites, while larger scales relate to clustering between isolated host halos.

We use the projected two-point correlation function, $w_p(r_p)$ because it does not suffer from peculiar velocities in the radial positions of galaxies. We present new measurements of the stellar mass clustering in DR7 based on our volume-limited catalogs, using the Landy–Szalay estimator (Landy & Szalay 1993). We use thresholds in stellar mass of $\log(M_*) > [10.6, 10.2, 9.8]$. The covariances are drawn from spatial jackknife sampling.

Measurement of $w_p(r_p)$ in the mock catalogs was done using the set of abundance matching models described in Section 3.2 applied to Bolshoi, with varying values of scatter and μ_{cut} . Because the simulation volume is similar to the volume of some of the volume-limited catalogs, it is important to understand the errors in the theoretical clustering measurements. The covariance matrices were estimated by finding the correlation function for each of a set of 300 PM simulations of the same volume as Bolshoi, but with the dark matter down-sampled to the same number density as the observed sample. These covariances were then scaled to the correlations measured on Bolshoi, according to

$$C_{B,ij} = C_{ij} \frac{w_{B,i} \times w_{B,j}}{\bar{w}_i \times \bar{w}_j}, \quad (1)$$

where C_B is the covariance matrix we use, and C that estimated from the multiple simulations. The w_B are the Bolshoi correlations, while \bar{w} is the mean from the simulations. The indices $[i, j]$ denote the bin. We use this procedure for each stellar mass threshold. We do not include any contributions from stellar mass errors in our errors on the correlation function.

4.2. Conditional Stellar Mass Function

The CSMF is the expected number of galaxies $\Phi(M_*|M_h)$ in a dark matter halo of mass M_h with a stellar mass of M_* .

An equivalent measure, the conditional luminosity function (CLF), carries similar information. The CSMF (or CLF) is a useful measurement for understanding both galaxy properties and cosmology (Yang et al. 2003, 2009; Cacciato et al. 2009; Hansen et al. 2009). A group catalog may be used to obtain the CSMF directly, by determining the mass of each group, then counting the galaxies in bins of stellar mass for each group mass. This allows direct counting of the number of galaxies in halos, independent of the clustering described above.

The CSMF may be split into two parts:

$$\Phi(M_*|M_h) = \Phi_c(M_*|M_h) + \Phi_s(M_*|M_h). \quad (2)$$

Here, Φ_c is the CSMF of central galaxies only, which are the individual galaxies at the center of each dark matter halo. Φ_c is a log-normal function. Φ_s is the CSMF of the satellite galaxies, and well approximated by a Schechter function. In the CLF, M_* may be replaced by L , the luminosity of the galaxies in the groups.

The same procedure is used on both the DR7 volume-limited catalog and the Bolshoi-based mock when measuring the CSMF. Comparisons are made in observational space, including the impacts of group finding. Errors are estimated in both cases by using bootstrap resampling of groups, with 100 samples.

4.3. Properties of Satellites and Centrals

We also investigate summary statistics of the CSMF. This includes the observed scatter in central galaxy stellar masses, as a function of group stellar mass. We also consider the satellite fraction in our models. We take this as the fraction of galaxies in our sample that are found to be satellites by the group finder, as a function of stellar mass.

4.4. Group Stellar Mass Function

The group stellar mass is the sum of the stellar masses of all galaxies in a group above some threshold in stellar mass, for each group. The least massive groups correspond to individual galaxies near the stellar mass threshold of $\log(M_*) > 9.8$, while the most massive correspond to clusters. The distribution of group stellar masses is the GSMF. The group luminosity function is the equivalent procedure, using luminosity rather than stellar mass.

5. UNDERSTANDING THE PARAMETERS

Before discussing explicit constraints on the parameters of the abundance matching models, it is helpful to consider the effect of varying each of them individually on the several measurements that we use. In Section 5.1, we consider varying the halo parameter used for abundance matching (Figure 4). In Section 5.2, we consider varying the scatter in stellar mass at a given halo property (Figure 5). In Section 5.3, we consider varying a the maximum amount halos can be stripped before galaxies are no longer identified (Figure 6).

5.1. Varying the Abundance Matching Parameter

The impact of varying the abundance matching parameter is shown in Figure 4. This figure shows the two-point correlation functions for three cuts in stellar mass and the CSMF in three bins of total stellar mass, which are later used to directly constrain the models. The satellite fraction, the scatter in the stellar mass of the central galaxy identified by the group finder, and the GSMF are also shown.

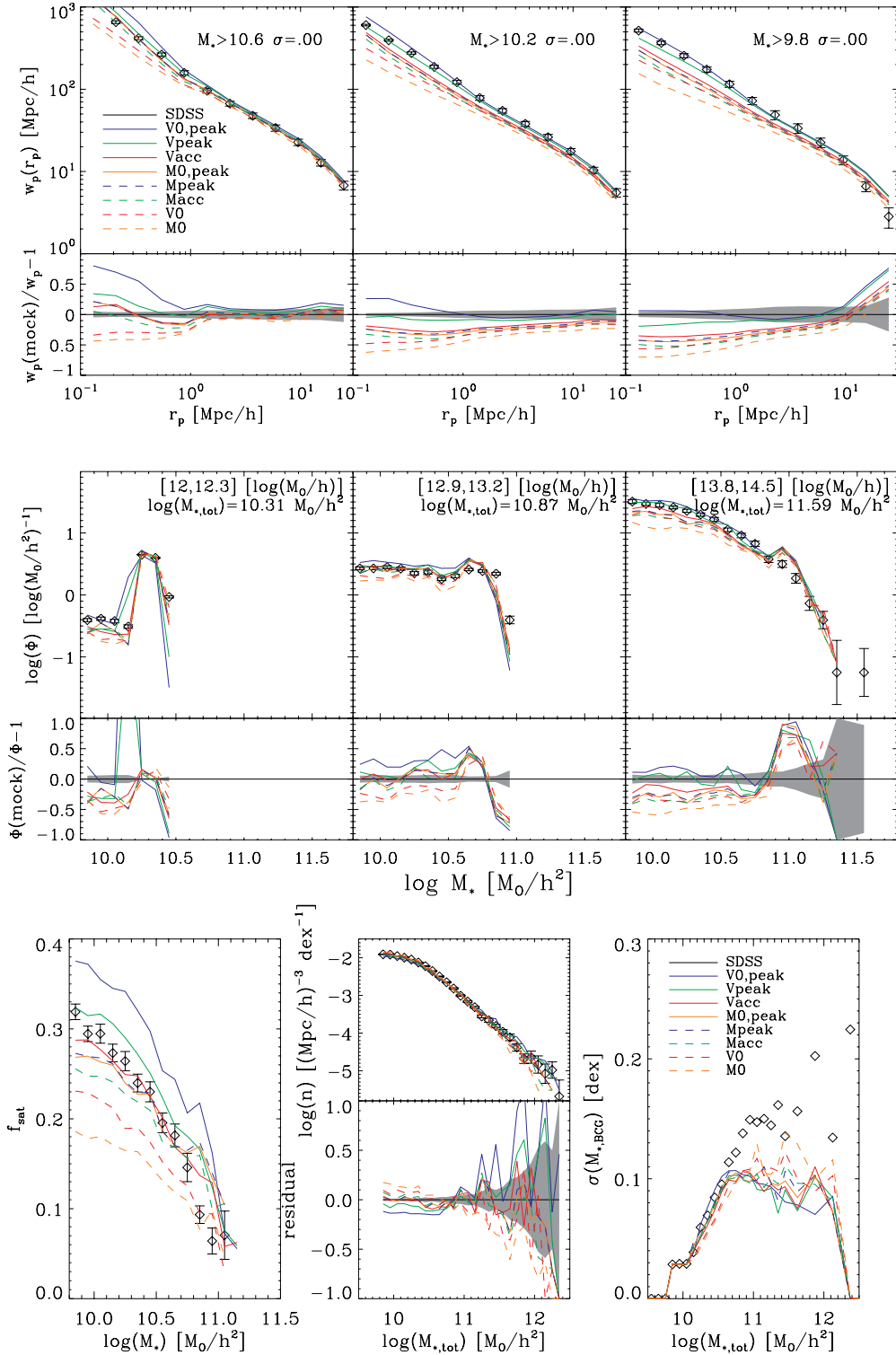


Figure 4. Statistical properties of galaxies as measured from simulated galaxy catalogs and galaxy group catalogs, constructed using different halo properties for abundance matching. All shown here have zero scatter and $\mu_{\text{cut}} = 0$. Top: projected two-point correlation function. Labels denote the stellar mass threshold, given in $\log(M_\odot h^{-2})$. Because increases in scatter or μ_{cut} can only decrease the clustering, it follows that any model which falls significantly below the measured clustering (black) must be excluded. Center: conditional stellar mass function (CSMF). Labels indicate the range in $\log(M_{\text{vir}})$ for each plot, as well as the median total stellar mass in each bin ($M_{*,\text{tot}}$). Nonzero scatter broadens this part of the distribution. Bottom left: satellite fraction as a function of stellar mass. As should be expected, models with higher satellite fraction also have stronger one-halo clustering and more satellites in the CSMF. Bottom center: group stellar mass function and residuals. Bottom right: standard deviation (scatter) in stellar mass of central as a function of total group stellar mass. The models are most readily distinguished by the small-scale clustering and changes in the satellite fraction. Error bars on the model points have been omitted for clarity.

(A color version of this figure is available in the online journal.)

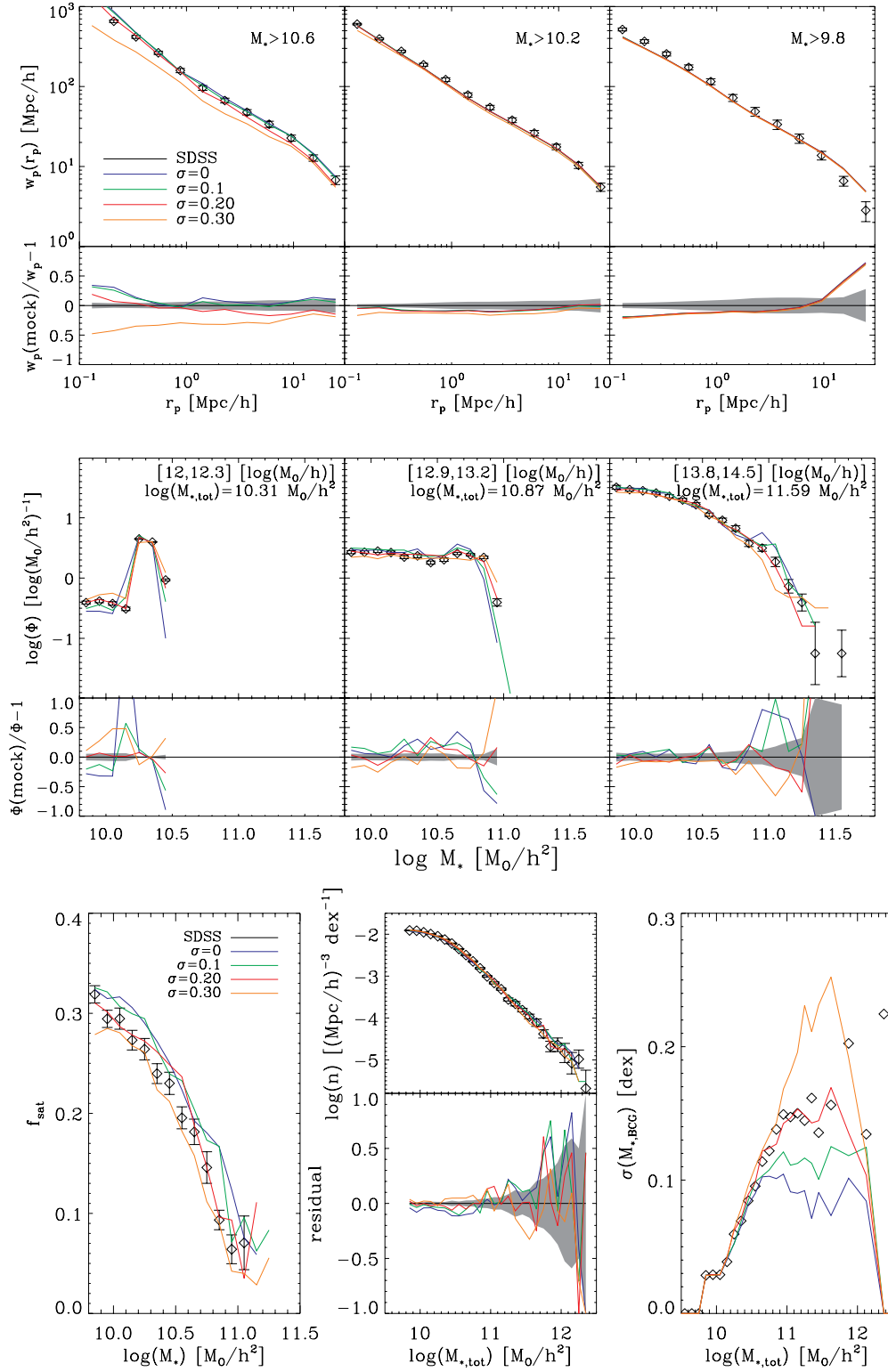


Figure 5. Impact of scatter in galaxy stellar mass at a given v_{peak} on observed statistics of the galaxy distribution. The models shown abundance match to v_{peak} with fixed $\mu_{\text{cut}} = 0$, with varying values of scatter. Increasing scatter reduces the clustering, but does not strongly affect clustering for thresholds below the characteristic stellar mass of the volume-limited sample. Individual plots are the same as described in Figure 4.

(A color version of this figure is available in the online journal.)

The impact of changing the abundance matching parameter on many of the results is best understood in the context of a halo occupation model. Correlations on small scales, below $\sim 1 \text{ Mpc h}^{-1}$, are determined by the distribution of galaxies in the same (host) halo, the one-halo term. Larger scales are

associated with the two-halo term, from the correlation between galaxies in different halos. For fixed values of scatter and μ_{cut} , the most significant effect of changing the parameter used in the abundance matching assignment is the change in the one-halo term. Changing the halo parameter used for abundance matching

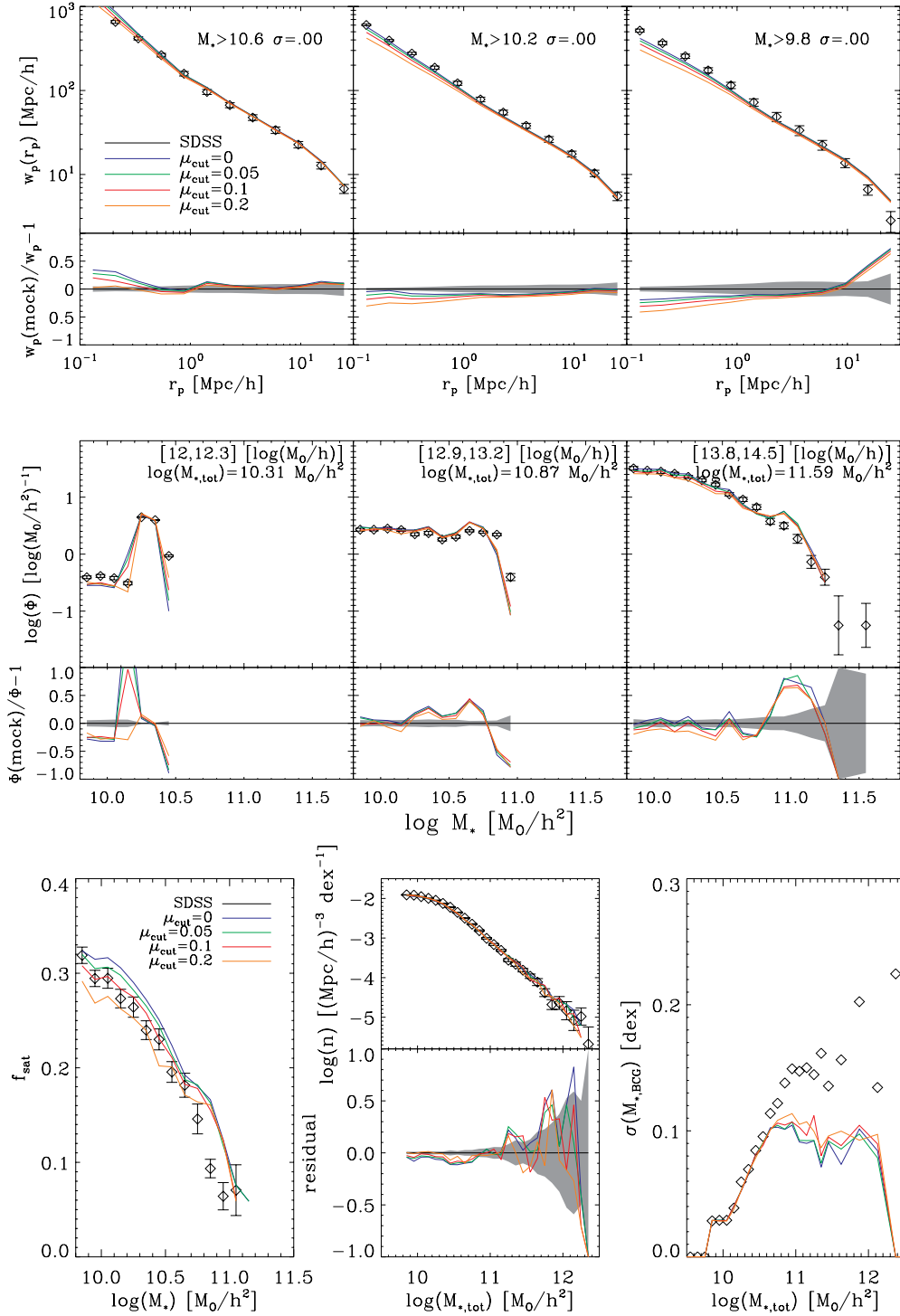


Figure 6. Impact of the μ_{cut} parameter, related to galaxy stripping, on observed statistics of the galaxy distribution. The models shown abundance match to v_{peak} with zero scatter in stellar mass, with varying values of μ_{cut} . Increasing μ_{cut} pushes down the clustering on small scales only, and decreases the satellite fraction. Individual plots are the same as described in Figure 4.

(A color version of this figure is available in the online journal.)

changes the relative circular velocities of halos and subhalos that are used to assign central and satellite galaxies, respectively. For example, the difference in the correlation function between v_{max} and v_{acc} is due primarily to the fact that subhalos are stripped after accretion. This difference can be seen in Figure 1 at $a = 1$: $v_{\text{acc}} > v_{\text{max}}$ for the example subhalo shown, but $v_{\text{acc}} = v_{\text{max}}$ for the distinct halo. Thus, when abundance matching to v_{acc} , this increases the fraction of galaxies that are satellites (hosted

by subhalos) at a fixed number density (and therefore above a fixed threshold in stellar mass) relative to the same procedure applied to v_{max} . This increase in number of satellites enhances the one-halo term due to additional satellites in clusters, but has little effect on the two-halo term.

The same pattern can be seen among all four different abundance matching methods using v_{max} . The parameter $v_{0,\text{peak}}$ results in the highest satellite fraction and the most small-scale

clustering. This is followed by v_{peak} and v_{acc} ; v_{max} the least clustered. A similar trend can be seen among the models using mass, though the differences tend to be smaller due to the smaller relative differences between mass definitions, as discussed in Section 3.2 and as can be seen for a pair of example halos in Figure 1. The mass-based matching is also less clustered than the equivalent v_{max} method; for example, v_{peak} is more clustered than M_{peak} . This is because, as shown in Figure 2, satellites tend to have higher v_{peak} than centrals at fixed M_{peak} . The results of all eight models with no scatter and $\mu_{\text{cut}} = 0$ are shown in Figure 4.

As is shown in the following two sections, using nonzero values of either scatter or μ_{cut} can only reduce the clustering, not increase it. Therefore, any model shown here that falls significantly below the measured projected correlation function cannot reproduce the clustering by any variation of these values, and is excluded from further consideration. This leaves only v_{peak} and $v_{0,\text{peak}}$ as viable models. Because these are the models with the highest values of the matching property for subhalos relative to distinct halos, this implies that stripping of the subhalo begins prior to the time of accretion, but that the stripping of the satellite galaxy it hosts does not begin until significantly later.

Our exclusion of all matching parameters other than v_{peak} and $v_{0,\text{peak}}$ is dependent on our particular abundance matching method. For example, we do not consider including “orphan” galaxies which may be present despite the disruption of their subhalos. We cannot rule out such models.

5.2. Varying Scatter

We evaluate the impact of scatter on galaxy statistics in Figure 5. For a fixed method of abundance matching, and fixed μ_{cut} , the effect of adding scatter is to reduce the clustering amplitude; this effect is most noticeable for the brightest, and most strongly biased, samples. This is due to the steepness of the SMF above the characteristic mass scale, where the falloff becomes exponential. It is more likely that less massive galaxies will be scattered to higher stellar mass than the reverse, decreasing the bias of galaxies above a fixed stellar mass threshold. However, this effect is reduced significantly for stellar mass thresholds less massive than this scale, since in this range the bias is only weakly mass dependent, and the SMF flattens.

Similarly, increasing the scatter directly broadens the central peak of the CSMF. In general, this scatter should increase the width of the stellar mass distribution of central galaxies in host halos of any mass. However, the assumption that the brightest galaxy is the central galaxy, combined with the use of the group finder, reduces this scatter dramatically in poorer groups. This effect is most striking in the smallest halos, where there may be one or no satellite galaxies, and the stellar mass of the central galaxy becomes directly related to the host halo mass determined by the group finder.

The scatter has some impact on the satellite portion of the CSMFs, tending to slightly reduce the number of satellites in clusters, and increase the number in small halos. This may be most easily understood by first considering the satellite fraction, which also tends to decrease at low stellar masses with increasing scatter.

More massive galaxies are more likely to be centrals because the fraction of halos of a given v_{max} which are subhalos generally decreases with v_{max} (or mass) (Kravtsov et al. 2004; Conroy et al. 2006). As scatter increases, this relationship weakens and the likelihood that a central galaxy is not the most massive galaxy—and therefore determined to be a satellite by the group

finder—should increase. That is, there is a significant likelihood that a satellite is more massive than the central in a particular host halo. The intrinsic satellite fraction of less massive galaxies should change only weakly with scatter, since most such low-mass galaxies are centrals with no satellites of sufficiently high stellar mass to scatter to a higher mass than the central. On the other hand, particularly in richer groups, some satellite galaxies will be scattered to higher stellar mass, possibly more massive than the true central. This suggests that the satellite fraction of low-mass galaxies should remain roughly constant with increasing scatter, and should increase at high stellar mass with increasing scatter. If this is surprising, consider the case of infinite scatter, where galaxy stellar mass is completely unrelated to the (sub)halo mass. In that case, the satellite fraction will be constant with stellar mass because satellites are as likely to be the most massive as centrals.

However, in the data, we do not know whether a galaxy is a central or satellite a priori. As a consequence, when the group finder assumes that the most massive galaxy is the central, it artificially reduces the satellite fraction of massive galaxies. Furthermore, this assignment changes the center of the measured halo away from the true center, which means that some galaxies that should be assigned as satellites are now outside the inferred virial radius. This tends to reduce the satellite fraction of low-mass galaxies. This same effect reduces the number of galaxies in massive clusters, as can be seen in the CSMFs.

The opposite effect is seen in the least-massive groups that we consider, where the number of satellites increases with scatter. This is due to our method of host mass assignment, where group stellar mass is used as the host mass proxy. When a small group, with one or no satellites, gains a new satellite above the stellar mass threshold due to scatter, the group will be pushed up in group stellar mass and added to the host mass selection. This effect is negligible on halos which host many satellites, which are dominated by the miscentering issue. (For more details, see Appendix A.)

The impact of scatter on the GSMF is also similar to that of μ_{cut} . That is, it increases the number of low stellar mass groups, and reduces the number of large clusters, steepening the GSMF.

In sum, increased scatter reduces the overall clustering amplitude, more strongly for higher stellar mass thresholds. It also broadens the central part of the observed CSMF in massive groups, and alters the shape of the observed satellite CSMF in a way that depends on the size of the group. The clustering prohibits high scatter, while the CSMF requires some moderate, nonzero scatter. The two parts of the CSMF provide the strongest constraint in this regard.

5.3. Varying μ_{cut}

Because μ_{cut} effectively removes satellites, and therefore most strongly affects small scales, it cannot be too large. Details of how μ_{cut} acts, however, depend somewhat on other details of the model in question. Figure 6 demonstrates the impact of μ_{cut} on our measurements.

To summarize the implications of these initial tests:

1. Any model, to reproduce the clustering, must have at least as many satellite galaxies as a model using v_{peak} as the abundance matching property. Of the set of properties we consider, only v_{peak} and $v_{0,\text{peak}}$ pass this criterion.
2. The μ_{cut} parameter most strongly affects small scales and the number of satellite galaxies, removing those whose subhalos were most stripped. To have enough satellite

Table 1
Quality of Fit

Model Type	μ_{cut}	σ (dex)	χ^2	N	$P(>\chi^2)$
v_{peak}	0.02	0.20	107	116	0.70
$v_{0,\text{peak}}$	0.15	0.24	260	116	$<10^{-4}$

galaxies to reproduce the clustering and CSMF, μ_{cut} cannot be too large.

- Increasing scatter reduces the clustering for the high stellar mass thresholds, widens the central CSMF distribution, and alters the shape of the satellite CSMF. It also reduces the satellite fraction. Scatter is most strongly constrained by the two parts, satellite and central, of the CSMF. Large scatter is also excluded by the two-point clustering measurements (zero scatter is only weakly disfavored by the clustering statistics alone).

6. CONSTRAINTS ON THE LOCAL GALAXY–HALO CONNECTION

6.1. Parameter Constraints

We now investigate the two candidate models which plausibly have enough substructure to match the data, abundance matching stellar mass to v_{peak} and $v_{0,\text{peak}}$. We systematically vary the parameters in these models to determine which are allowed by the data. For each model, we consider a large grid of models in the scatter and μ_{cut} parameters described above, and evaluate which range in these parameters provides an acceptable fit to the correlation function and the CSMF measured in the SDSS data.

At every point in parameter space, we measure the CSMF after passing the mock catalog through the group-finding procedure and add fiber collisions, as discussed in Section 3. This ensures that we accurately mimic the systematic effect these have on the galaxy groups. Additionally, we add a systematic error to account for shot noise in the galaxy assignment, which is due to using a finite number of halos. For a fixed set of model parameters, we produced 25 mock catalogs. Though these have the same input parameters and SMF, the stochasticity of the algorithm produces a certain amount of variation between individual implementations. We estimated the point-by-point variation between these models for all the measures we use to constrain the fit, and add this estimated variance to the diagonals of the covariance matrices. Table 1 lists the overall fit results for v_{peak} and $v_{0,\text{peak}}$, including this systematic error. (Unless otherwise noted, error bars shown in plots are statistical only.) Systematic errors are of roughly the same magnitude as the statistical errors. There is no large change in our conclusions when we do not include these systematic errors.

To fully accommodate the variation between individual implementations of any given model, we take the mean of each data point and all of its neighbors in parameter space, and the mean variances. For instance, for a point at $\mu_{\text{cut}} = 0.02$ and $\sigma = 0.20$, we take the mean CSMF and two-point clustering of the nine data points within $\mu_{\text{cut}} = 0.02 \pm 0.01$ and $\sigma = 0.20 \pm 0.01$. This is a reasonable procedure as nearby points in parameter space have relatively small changes in output observables and it smooths fluctuations in the likelihood due to occasional individual outlier points in the CSMF.

We find that only the model based on v_{peak} can produce an adequate fit to both the CSMF and the clustering combined.

This model provides an excellent fit to the CSMF and clustering above $\log(M_*) \sim 10$. However, in general, even the best-fit versions have slightly low clustering on small scales for the $\log(M_*) > 9.8$ samples. Because we cannot cleanly determine whether this is due to a systematic issue with the simulation or a problem with the model, we exclude this lowest threshold from the total χ^2 calculated for the combined measures. The $M_h = [12.6, 12.9]$ host mass bin from the CSMF estimated χ^2 , has significant fluctuations in neighboring bins in stellar mass, which suggest some problematic behavior in the SDSS measurement in that bin, and we omit this bin from our combined fits.

Parameter constraints for this model are shown in Figure 7. Here we show the constraints from clustering alone, from the central and satellite parts of the CSMF separately, and from all of these statistics together. Notably, all three data sets require scatter of <0.25 dex. Marginalizing over scatter to obtain μ_{cut} provides only upper limits: $\mu_{\text{cut}} < 0.07$ (68%) and $\mu_{\text{cut}} < 0.11$ (95%). Marginalizing over μ_{cut} and interpolating between points in parameter space, the resulting constraints on scatter using the v_{peak} model are $\sigma = 0.200 \pm 0.02$ dex (68%) or $\sigma = 0.200 \pm 0.03$ dex (95%). The scatter is most strongly constrained by the two components of the CSMF, while μ_{cut} is determined largely by the clustering.

The measured statistics of the best-fit model are shown in Figure 8. For the best-fit case, we use scatter of 0.20 dex, and $\mu_{\text{cut}} = 0.03$, both well inside the constraints. This is the best-fit model in the absence of the local averaging procedure described above for estimating the constraints. We show the clustering and stellar mass functions used to constrain the model, which are in excellent agreement except for the dimmest galaxies. We also compare the total GSMF, the satellite fraction, and the scatter in central galaxy properties. All statistics are in excellent agreement with the data for galaxies with stellar masses greater than $\log(M_*) \sim 10$; there is slightly less clustering and a smaller substructure fraction in the lowest bin of stellar mass.

As shown in Figure 7, both the central and satellite parts of the CSMF constrain the scatter in stellar mass at fixed (sub)halo mass in our model. To check our assumption that scatter is constant with respect to (sub)halo v_{peak} , we can obtain the best fit in each bin in inferred host halo mass, or total group stellar mass, which is strongly correlated with v_{peak} . This result is shown in Figure 9. Here we are using the CSMF only (and not the clustering), and use the results from the mass bins independently, thus the constraints at a given mass are weaker than the full model constraint. However, it is clear that a scatter of 0.20 dex is in excellent agreement with the result in each individual mass bin, within the 68% bounds, after marginalizing over μ_{cut} . A very mild trend in the scatter parameter with mass would still be consistent with these constraints.

The low clustering for the dimmest sample considered implies that the model catalogs are missing dim satellites in general; a deficit of satellites in groups and clusters will reduce the small-scale clustering. A hint of this is also visible in the satellite fraction, which is slightly low in the lowest stellar mass bin. Further hints are seen in the radial profiles of galaxies, which show a slight deficit in the density of galaxies in the innermost regions (see Appendix E). It is possible that this is due to a lack of resolution in the N -body simulation on the smallest scales, which could artificially destroy subhalos that correspond to these galaxies. Equivalently, this may imply support for the inclusion of “orphan” galaxies, which still exist yet whose dark matter halos have already been significantly disrupted (see,

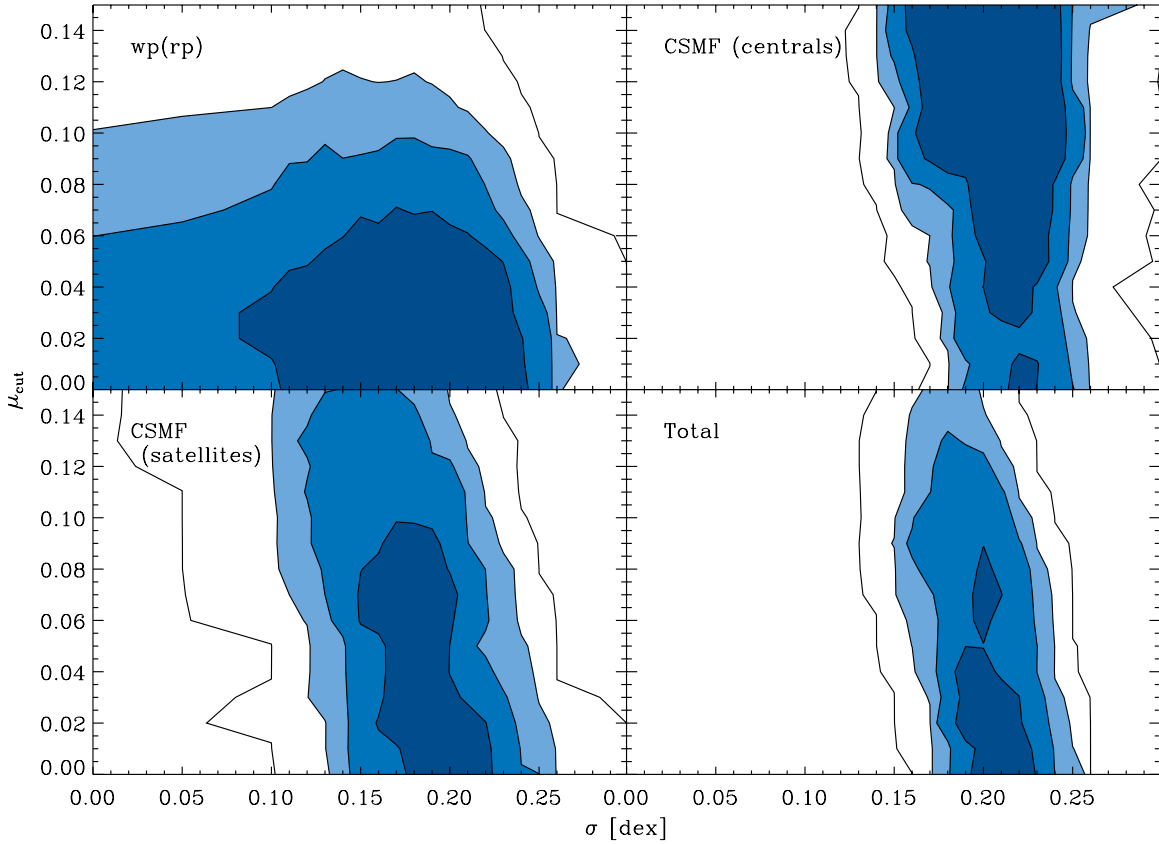


Figure 7. Constraints for the scatter and μ_{cut} parameters, for abundance matching models which assign galaxies to v_{peak} of both halos and subhalos. Clustering constraints use data for galaxies with $\log(M_*) > 10.2$. Levels give $P(>\chi^2)$, corresponding to 1σ , 2σ , 3σ , and 5σ contours. Upper left: constraint from clustering only. Upper right: constraint from central part of CSMF only. Lower left: constraint from satellite part of CSMF only. Lower right: parameter constraints using the total χ^2 from all three measurements.

(A color version of this figure is available in the online journal.)

e.g., Guo et al. 2011 and references therein for a discussion of orphans). Adding a small number of orphan galaxies may be able to correct the correlation function without significantly increasing the number of satellites. Alternatively, it is possible that some form of assembly bias becomes important at low stellar masses, or that the μ_{cut} parameter varies with stellar mass. A model similar to the last suggestion was considered by Watson et al. (2012) and found to provide a good match. However, these possibilities are degenerate and we postpone a full consideration of these degeneracies to future work. We note that for the Bolshoi simulation considered here, there is no indication that orphans, assembly bias, or non-constant parameters are required for galaxies with $\log(M_*) > 10$.

We find that the $v_{0,\text{peak}}$ model is not able to provide an acceptable fit to the data for any region in parameter space. With respect to the correlation function alone, $v_{0,\text{peak}}$ is capable of matching or exceeding the correlation function in all bins, as shown in Figure 4 and with the $w_p(r_p)$ constraint shown in Figure 10. In fact, only the $v_{0,\text{peak}}$ model can produce a good fit to all three stellar mass thresholds simultaneously. However, it is not able to match either the central or satellite portions of the CSMF. The central portion of the CSMF is offset somewhat low in stellar mass, due to the increased number of bright satellites. The high scatter and μ_{cut} needed to match the width of the central CSMF and the high stellar mass w_p also reduces the number of satellites too much for both the central and satellite parts of the CSMF to be fit simultaneously. Although this model is ruled out by the data, the values with the best fit for the $v_{0,\text{peak}}$ matching parameter are $\mu_{\text{cut}} \sim 0.14$ and scatter of ~ 0.24 dex.

6.2. Halo Properties for Satellite and Central Galaxies in the Best-fit Model

The results shown in the previous section were all in observed space. We now consider the properties of the underlying model in our best-fit case. For the best-fit case, we use scatter of 0.20 dex, and $\mu_{\text{cut}} = 0.03$, both well inside the constraints. This is the best-fit model in the absence of the local averaging procedure described above for estimating the constraints.

A series of general relationships between halo (or subhalo) properties and galaxy stellar mass for our best-fit model are shown in Figure 11. This shows the median values of various halo properties in bins of stellar mass, split between satellite and central galaxies. The relationship between v_{peak} and stellar mass is nearly the same for both satellites and centrals. This is as expected, since when abundance matching stellar mass to halos sorted by v_{peak} we make no distinction between satellites and centrals.

On the other hand, the satellite galaxies have significantly lower v_{max} at the present time. This is sensible, as (sub)halos with the same v_{peak} host galaxies with comparable stellar mass, but satellite galaxies at that same stellar mass are in subhalos with lower v_{max} due to stripping following accretion. As a result, central galaxies with $\log(M_*) < 10.5$ are in halos with roughly 25% higher v_{max} than subhalos hosting satellite galaxies with the same stellar mass. This difference increases to as much as $\sim 35\%$ at higher stellar mass. This result may be in tension with a recent study of the variation of the Tully–Fisher relation on environment using SDSS galaxies (Mocz et al. 2012),

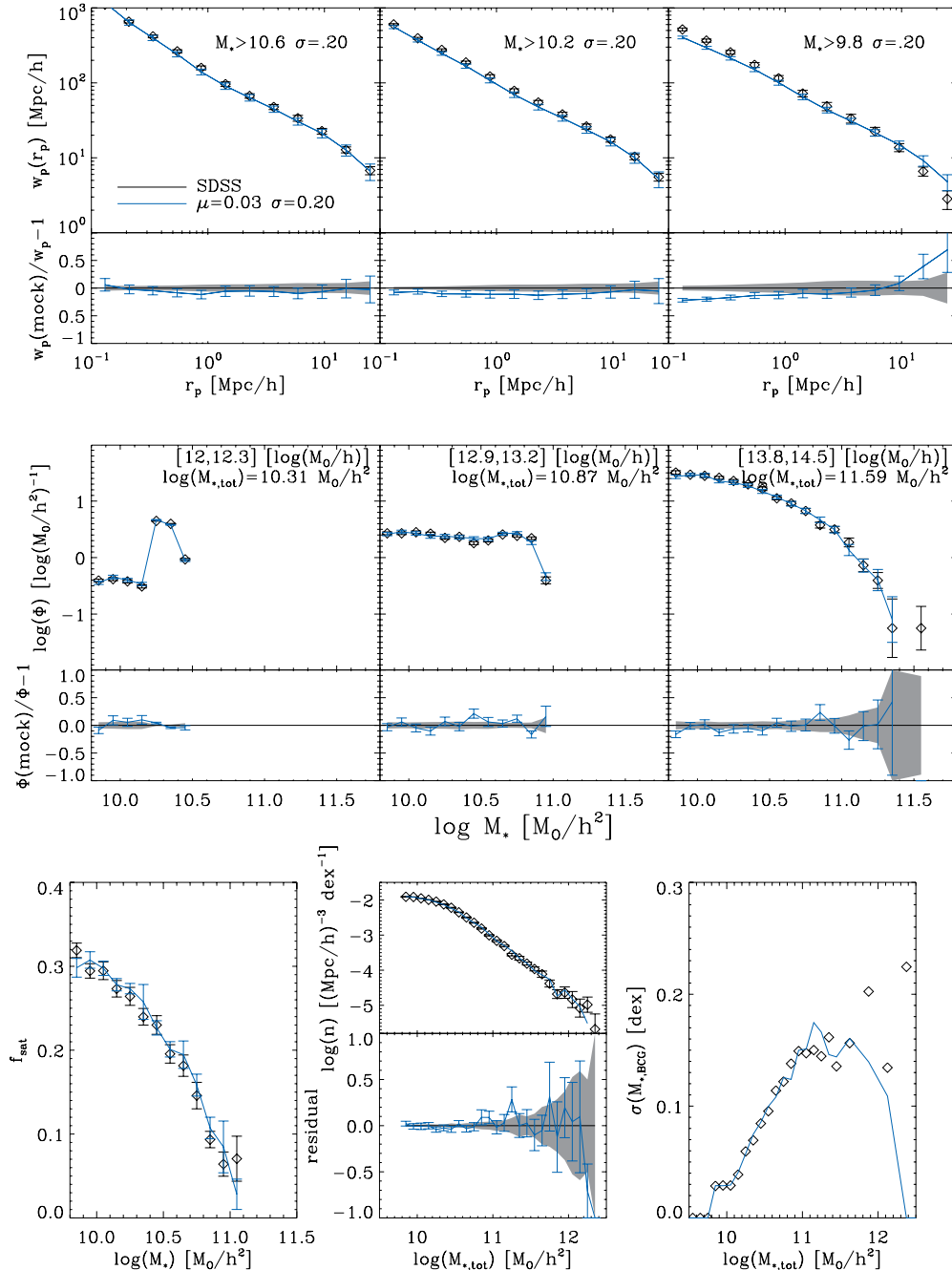


Figure 8. Comparison of observed galaxy statistics between SDSS DR7 and our best-fit model, which uses v_{peak} , $\mu_{\text{cut}} = 0.03$ and scatter = 0.20 dex. Note that only the CSMF and correlation functions with $\log(M_*) > 10.2$ are used for fitting. Plots are the same as described in Figure 4.

(A color version of this figure is available in the online journal.)

which finds no dependence on environment. However, a direct comparison is complicated by differences in the environment definition from our designation of central and satellite galaxies, as well as differences in sample selection, so we leave a precise comparison to future work.

It is also noteworthy that for (sub)halos hosting lower stellar mass galaxies, the subhalos have a much larger variation in v_{max} than do the distinct halos. This is due to the wide variety in v_{max} that may be associated with the same past v_{peak} , depending on how much the individual subhalo has been stripped since it was accreted.

The distribution of galaxies in the host halo mass at a fixed stellar mass is an interesting complement to the CSMF. As one

might expect, satellite galaxies (and their subhalos) tend to be hosted by significantly more massive distinct halos than central galaxies of the same stellar mass. The variation in satellites' host masses is also much larger at lower stellar mass, since a relatively small subhalo may reside in a low-mass halo, as well as a very massive dark matter halo. At higher stellar mass, this relationship narrows, since only sufficiently massive dark matter halos can host massive subhalos, and, hence, very massive satellite galaxies. We refer to this host mass, of the distinct halo containing a central or both a satellite and its subhalo, as M_{host} .

The variation in v_{peak} , v_{max} , or M_{host} at fixed central stellar mass is reduced as stellar mass decreases. This is most likely

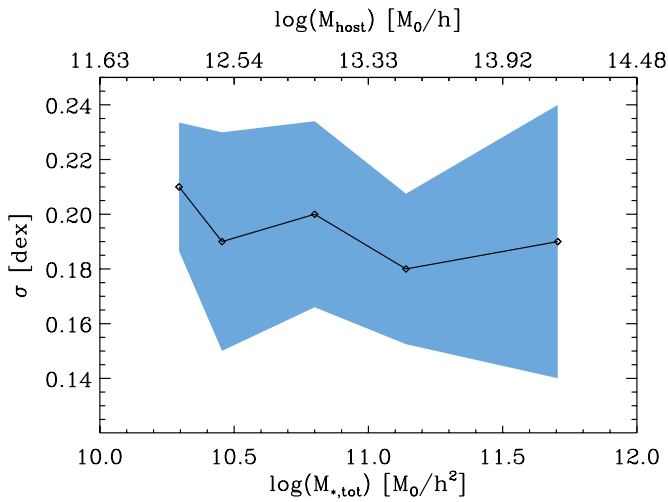


Figure 9. Maximum likelihood (black points) value of the scatter in each bin in inferred host halo mass, marginalized over μ_{cut} , using constraints from the conditional stellar mass function alone. Gray bands show the 68% bounds. The scatter value is consistent with our overall best-fit scatter of 0.20 dex in the full mass range from 10^{12} to 10^{14} .

(A color version of this figure is available in the online journal.)

due to the fact that at high stellar mass, the SMF, as well as the halo mass function and the circular velocity function, is much steeper. Thus, at high stellar masses, a bin of fixed width yields a wider range of values in the circular velocities or host halo mass.

6.3. Best-fit Conditional Stellar Mass Function

Following Yang et al. (2009) and Cacciato et al. (2009), we fit the central galaxies with a log-normal function. We find that a Schechter function is sufficient for the satellite galaxies (as has been found previously; see, e.g., Moster et al. 2010). When we perform fits to the CSMF, we adopt the following parameterization of these quantities, using in all cases the differential $d \log(M_*)$:

$$\Phi_c(M_*|M_{\text{host}}) = \frac{1}{\sqrt{2\pi}\sigma_c} \exp\left(-\frac{(\log M_* - \log M_{*,c})^2}{2\sigma_c^2}\right) \quad (3)$$

$$\Phi_s(M_*|M_{\text{host}}) = \phi_* \left(\frac{M_*}{M_{*,s}}\right)^{\alpha+1} \exp\left(-\frac{M_*}{M_{*,s}}\right). \quad (4)$$

Thus, the central galaxies are characterized by two parameters: $M_{*,c}$, which is the geometric mean of the central stellar mass, and σ_c , which is the width of the log-normal distribution in dex. Both are closely related to the scatter in the model, as described below. The satellite galaxies are described by the usual three parameters of a Schechter function. Here, $M_{*,s}$ is the cutoff luminosity, α the faint-end slope, and ϕ_* the overall normalization. Unlike in Yang et al. (2008, 2009), we choose not to fix the relationship between $M_{*,c}$ and $M_{*,s}$ explicitly. These results are compared to others in the literature in Section 7.

The results of fitting to the intrinsic CSMF can be seen in Figure 12. This is the CSMF in the Bolshoi simulation, using our best-fit model, and without observational complications (e.g., group finding). Here, a galaxy is a satellite if its halo is a subhalo. This is the same model as shown in Figure 8; the main difference between the two is that the intrinsic CSMF does not require that the central galaxy has the most stellar

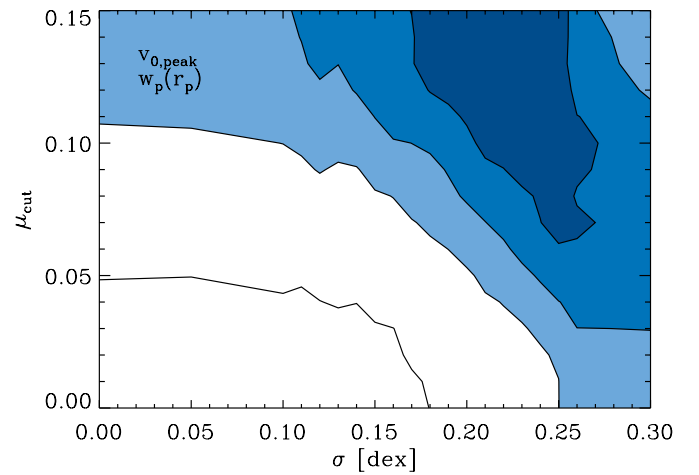


Figure 10. Same as Figure 7, but using $v_{0,\text{peak}}$, and using data for galaxies with $\log(M_*) > 10.2$. Levels give $P(>\chi^2)$, corresponding to 1σ , 2σ , 3σ , and 5σ contours. The only constraint plot shown is that for the two-point correlation function. The CSMFs have such high χ^2 values that they are all completely excluded over this parameter space at the 5σ level.

(A color version of this figure is available in the online journal.)

mass, a necessary assumption of the group-finding algorithm. This produces the sharp central peak that can be seen in Figure 8 and the other comparison figures. However, as can be seen in Figure 12, the underlying distribution is much broader. This is primarily due to the 0.20 dex scatter in this model, with a small contribution from the finite size of the mass bin.

A few additional intrinsic measurements are shown in Figures 13 and 14. For all of these plots, we extrapolate our SMF down to stellar masses of $10^8 M_\odot h^{-2}$. Figure 13 shows the intrinsic satellite fraction and scatter, which may be contrasted with the mock observed values in Figure 8. Notably, in the intrinsic case, the satellite fraction flattens below the cutoff stellar mass of $\log(M_* h^2/M_\odot) = 9.8$ in our volume-limited sample. The scatter in central stellar mass at fixed group total stellar mass shows the same trend as in the observed case, with low scatter at low stellar masses due to the fact that the central contributes nearly all of the stellar mass. However, because no group finding is involved to artificially reduce the scatter for groups with many galaxies, it reaches ~ 0.2 dex at the massive end.

We also show the more finely binned trends in the characteristic group stellar mass, central galaxy stellar mass, and satellite galaxy stellar mass in Figure 14. At low host masses, there are few satellite galaxies with even $10^8 M_\odot h^{-2}$ solar masses, and so the measured $M_{*,s}$ is not reliable below $\log M_{\text{host}} \sim 11.5$. The central stellar mass and satellite stellar mass $M_{*,s}$ are only slowly changing for host halo masses above $\sim 10^{13} M_\odot h^{-1}$, and then fall off at lower host halo masses. Note that the ratio between central galaxy stellar mass and satellite stellar mass $M_{*,s}$ is roughly constant over a broad range in host halo mass, which is in general agreement with results from Yang et al. (2009). This figure includes some of the results of a fit parameterized to host halo mass, which works well for $M_{\text{host}} > 10^{12} M_\odot h^{-1}$ and is discussed in the next section.

6.4. Conditional Stellar Mass as a Function of Halo Mass

To more generally describe the CSMF, we take the parameters from Equations (3) and (4) to be functions of host halo mass.

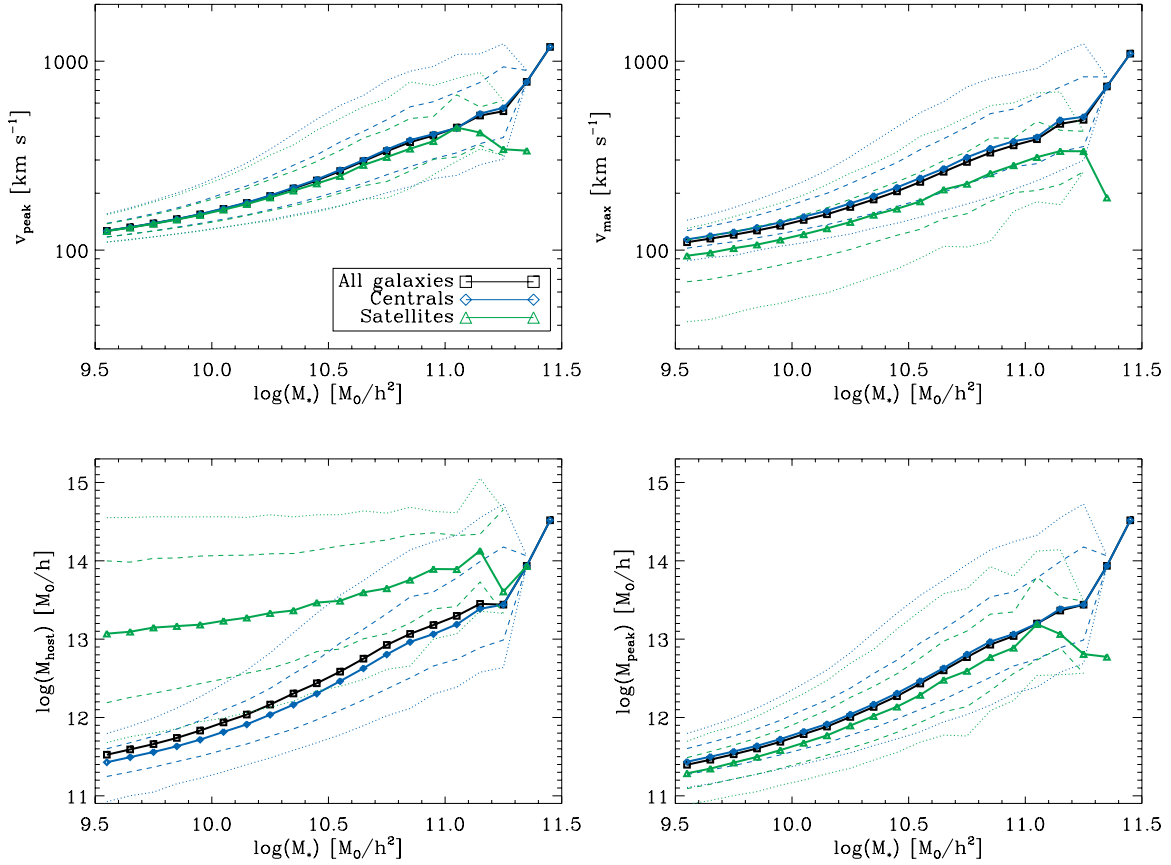


Figure 11. M_* relationship with v_{peak} (top left), v_{max} (top right), host halo mass (bottom left), and peak (sub)halo mass (bottom right) for the best-fit model, with matching based on v_{peak} , with 0.20 dex scatter and $\mu_{\text{cut}} = 0.03$. Blue indicates centrals, green, satellites. Solid black lines are the median of the total (satellites plus centrals). Solid lines are the median values of v_{max} or v_{peak} for bins in M_* . Dashed and dotted lines contain given the 68% and 95% bounds on galaxies in each bin, centered at the median. Although the central and satellite distributions are similar in v_{peak} due to how the catalog is constructed, satellites typically have lower v_{max} and larger dispersion due to stripping after accretion. (All units are given with $h = 1$.)

(A color version of this figure is available in the online journal.)

For the central CSMF, the mean stellar mass is defined by

$$\log(M_{*,c}) = \log(M_0) + g_1 \log\left(\frac{M_{\text{host}}}{M_1}\right) + (g_2 - g_1) \log\left(1 + \frac{M_{\text{host}}}{M_1}\right), \quad (5)$$

where M_0 is a characteristic stellar mass, M_1 is a characteristic host halo mass, and g_1 and g_2 are power-law slopes. M_h is the host halo mass. The width σ_c of the log-normal function is assumed to be constant as a function of host halo mass.

The satellite CSMF is determined by the three Schechter function parameters, ϕ_* , α , and $M_{*,s}$:

$$\phi_* = \left(\frac{M_{\text{host}}}{M_\phi}\right)^a \quad (6)$$

$$\log(M_{*,s}) = \log(M_{*,0}) + b \log\left(\frac{M_{\text{host}}}{M_{*,1}}\right) - b \log\left(1 + \frac{M_{\text{host}}}{M_{*,1}}\right). \quad (7)$$

The slope α is assumed to be constant as a function of halo mass. Based on Figure 12 and the individual fit results in Table 2, it is evident that α varies significantly from one fit to another without a commensurate variation in the shape of the satellite

CSMF. This is due to the fact that when limiting the fit to stellar masses $\log(M_*) > 9.8$ we lose constraining power on the low-mass slope, and it becomes degenerate with the other satellite parameters. When we consider the extrapolation to lower stellar mass, we find that the slope at all host masses converges to $\alpha \sim -1$. There, we hold $\alpha = -1$ fixed.

We then fit this functional form to the binned CSMF data. The parameters for the resulting fit are in Tables 4 and 5 for the DR7 input SMF. The overall result of this fit is shown in Figure 15, which clearly reproduces the data well. Some comparisons of the parameters as a function of halo mass are shown in Figure 14 as discussed in the previous section.

6.5. Best-fit Halo Occupancy Distribution

The HOD may be used, for instance, to predict or fit to galaxy clustering (Zheng et al. 2007; Watson et al. 2011; Zehavi et al. 2011). The HOD is defined in part by $P(N|M_h)$, the probability of finding N galaxies of some type in a halo of mass M_h . The common procedure takes galaxies brighter than some fixed stellar mass $M_{*,\text{min}}$ as the type of interest. In this case, the expectation of the HOD may be obtained directly from the CSMF:

$$\langle N(M_{\text{host}}) \rangle = \int_{M_{*,\text{min}}}^{\infty} \Phi(M_*|M_{\text{host}}) dM_*. \quad (8)$$

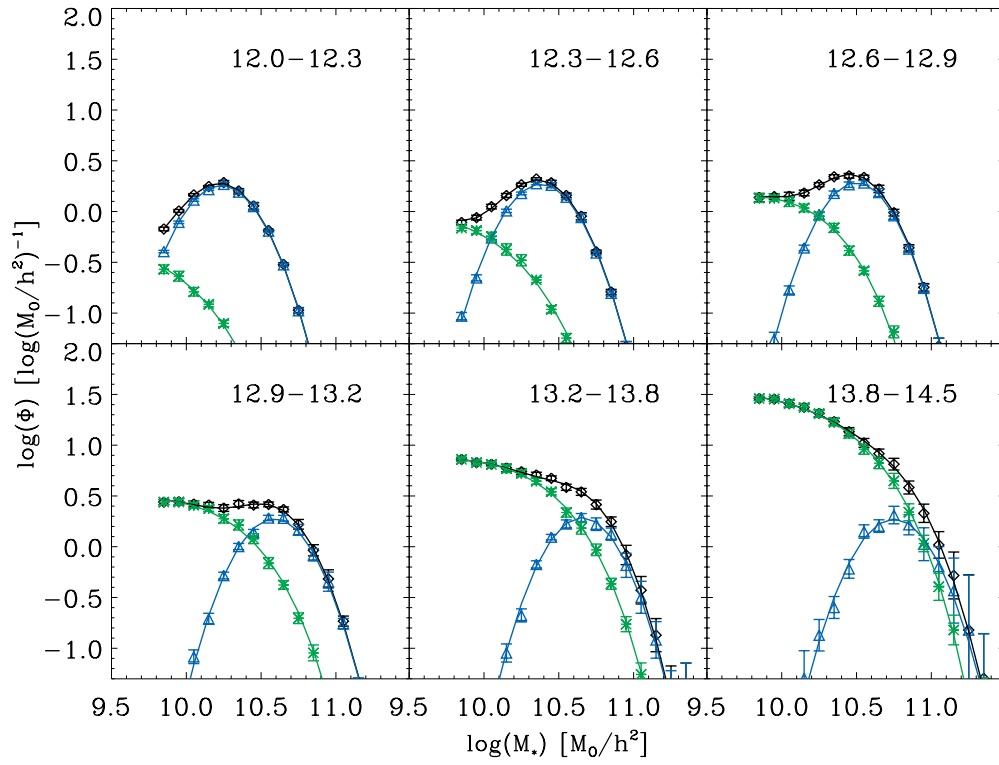


Figure 12. CSMF fits for the best model. Black is the overall CSMF; blue, central galaxies only; green, satellite galaxies only. Solid lines are the respective fits. Labels give the host mass range in $\log(M_{\odot} h^{-1})$. Equations (3) and (4) describe the fit, while Table 2 lists the parameters. Error bars include estimated systematic errors. (A color version of this figure is available in the online journal.)

Table 2
Intrinsic CSMF Fit Parameters for Best-fit Model

M_{host} ($\log(M_{\odot} h^{-1})$)	$\log(M_{*,c})$ ($\log(M_{\odot} h^{-2})$)	σ_c ($\log(M_{\odot} h^{-2})$)	ϕ_* ($\log(M_{\odot} h^{-2})^{-1}$)	α	$\log(M_{*,\text{Sch}})$ ($\log(M_{\odot} h^{-2})$)	No. of Hosts
12.0–12.3	10.232 ± 0.001	0.218 ± 0.001	0.652 ± 0.059	-0.98 ± 0.16	9.92 ± 0.04	27948
12.3–12.6	10.383 ± 0.002	0.212 ± 0.001	1.56 ± 0.08	-0.76 ± 0.10	10.01 ± 0.02	14983
12.6–12.9	10.500 ± 0.002	0.205 ± 0.001	3.40 ± 0.09	-0.41 ± 0.08	10.04 ± 0.02	7814
12.9–13.2	10.591 ± 0.003	0.209 ± 0.002	6.07 ± 0.22	-0.62 ± 0.06	10.17 ± 0.02	4000
13.2–13.8	10.656 ± 0.004	0.206 ± 0.002	13.5 ± 0.5	-0.74 ± 0.04	10.27 ± 0.01	2896
13.8–14.5	10.748 ± 0.009	0.213 ± 0.004	42.5 ± 2.3	-0.95 ± 0.05	10.38 ± 0.02	595

Table 3
Intrinsic HOD Fit Parameters for Best-fit Model

M_* Threshold ($\log(M_{\odot} h^{-1})$)	$(M_r - 5 \log(h))$	$\log(M_{\text{min}})$ ($\log(M_{\odot} h^{-1})$)	σ_m ($\ln(M_{\odot} h^{-1})$)	$\log(M_1)$ ($\log(M_{\odot} h^{-1})$)	$\log(M_{\text{cut}})$ ($\log(M_{\odot} h^{-1})$)	α_{HOD}	No. of Galaxies
10.76	-21.5	13.71 ± 0.03	2.30 ± 0.06	14.31 ± 0.13	13.1 ± 0.5	0.97 ± 0.30	4437
10.54	-21.0	12.924 ± 0.006	1.75 ± 0.01	13.74 ± 0.15	12.8 ± 0.3	0.94 ± 0.21	18062
10.31	-20.5	12.318 ± 0.002	1.161 ± 0.002	13.30 ± 0.17	12.6 ± 0.2	0.93 ± 0.17	49715
10.07	-20.0	11.950 ± 0.001	0.9000 ± 0.0007	12.98 ± 0.18	12.4 ± 0.2	0.94 ± 0.15	103904
9.82	-19.5	11.6336 ± 0.0001	0.6248 ± 0.0001	12.76 ± 0.17	12.2 ± 0.2	0.95 ± 0.13	174932
9.54	-19.0	11.4588 ± 0.0002	0.6047 ± 0.0001	12.59 ± 0.16	12.0 ± 0.2	0.96 ± 0.11	261915

Table 4
CSMF Mass-dependent Fit Parameters—Centrals

SMF	$\log(M_0)$ ($\log(M_{\odot} h^{-2})$)	$\log(M_1)$ ($\log(M_{\odot} h^{-1})$)	g_1	g_2	σ_c ($\log(M_{\odot} h^{-2})$)
VAGC	10.64 ± 0.03	12.59 ± 0.10	0.726 ± 0.055	0.065 ± 0.021	0.212 ± 0.001
Y09	10.96 ± 0.05	12.94 ± 0.12	0.644 ± 0.028	0.155 ± 0.031	0.215 ± 0.001
B12	10.77 ± 0.01	12.40 ± 0.05	0.947 ± 0.061	-0.003 ± 0.003	0.213 ± 0.001
M12	10.56 ± 0.07	12.21 ± 0.20	1.19 ± 0.26	0.224 ± 0.017	0.218 ± 0.002

Table 5
CSMF Mass-dependent Fit Parameters—Satellites

SMF	$\log(M_{*,0})$ ($\log(M_{\odot} h^{-2})$)	$\log(M_{*,1})$ ($\log(M_{\odot} h^{-1})$)	b	$\log(M_{\phi})$ ($\log(M_{\odot} h^{-1})$)	a
VAGC	10.401 ± 0.008	12.71 ± 0.08	0.753 ± 0.063	12.30 ± 0.01	0.866 ± 0.010
Y09	10.664 ± 0.008	12.60 ± 0.07	0.948 ± 0.083	12.42 ± 0.01	0.881 ± 0.006
B12	10.538 ± 0.006	12.35 ± 0.09	1.26 ± 0.16	12.43 ± 0.01	0.951 ± 0.007
M12	10.553 ± 0.009	12.65 ± 0.08	0.986 ± 0.092	12.41 ± 0.01	0.875 ± 0.007

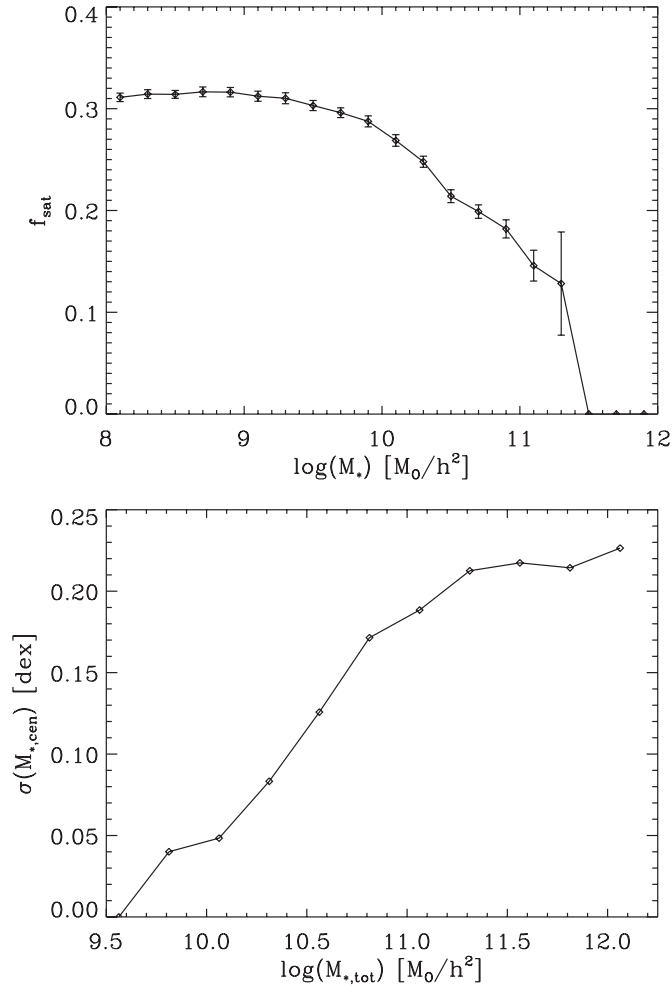


Figure 13. Additional measures of the intrinsic distribution of galaxies in our best-fit model. Top: intrinsic satellite fraction as a function of stellar mass. Because the input SMF only extends down to $\log(M_*) = 9.8$, stellar masses below this cutoff are drawn from a power-law extrapolation to the input SMF. Bottom: scatter in central galaxy stellar mass as a function of total group mass. Note the difference between the intrinsic scatter shown here and the smaller “observed” scatter after group finding shown in Figure 8. In both cases, this scatter becomes poorly defined for groups with no galaxies above the stellar mass cutoff.

Similar to the CSMF, the HOD may also be split into central and satellite contributions, with $\langle N(M) \rangle = \langle N_c \rangle + \langle N_s \rangle$. The central portion may be described by a step function, with a cutoff of some width. Thus, there is some minimum host mass, M_{\min} , below which the halo is too small to host a central galaxy brighter than $M_{*,\min}$. Above M_{\min} , each halo typically hosts one central galaxy; below M_{\min} , each typically hosts none. The satellite galaxies are a different matter, generally well described by a power law, with some cutoff at or above M_{\min} . Below this cutoff there are very few satellite galaxies.

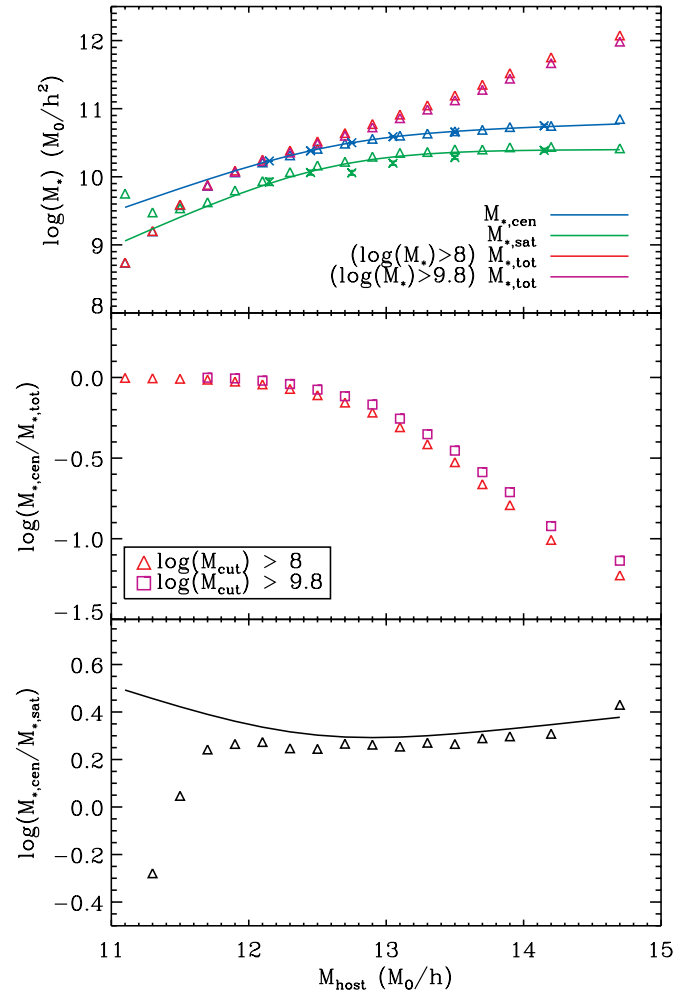


Figure 14. Measures of the intrinsic distribution of galaxies in our best-fit model. Top: median central mass ($M_{*,c}$), median total group stellar mass ($M_{*,tot}$) for two different stellar mass thresholds, and the fitted $M_{*,s}$ to a Schechter function in narrow mass bins (triangular points). Solid lines are the fitted values of $M_{*,c}$ and $M_{*,s}$ as discussed in Section 6.4. The x’s with error bars indicate the $M_{*,c}$ and $M_{*,s}$ fitted values in the individual mass bins used for observational comparisons. Center: ratio of the median central stellar mass to the median total group stellar mass, as a function of host halo mass. This becomes less meaningful as the central comes to dominate the group’s stellar mass. Bottom: ratio of characteristic satellite stellar mass $M_{*,s}$ to the median central stellar mass. Note that this is fairly constant at $\log(M_{*,c}/M_{*,s}) \sim 0.28$. The solid line indicates the difference in the host mass dependent fits for $M_{*,c}$ and $M_{*,s}$. In all cases, cuts in stellar mass are given in $\log(M_{\odot} h^{-2})$.

(A color version of this figure is available in the online journal.)

While the usual approach to determining the HOD is to perform a fit to the clustering and number density data, we instead use the information on group association available in the simulations to measure the HOD directly. This is done by counting all galaxies above some stellar mass for each (host) halo of a given mass, then averaging over all halos.

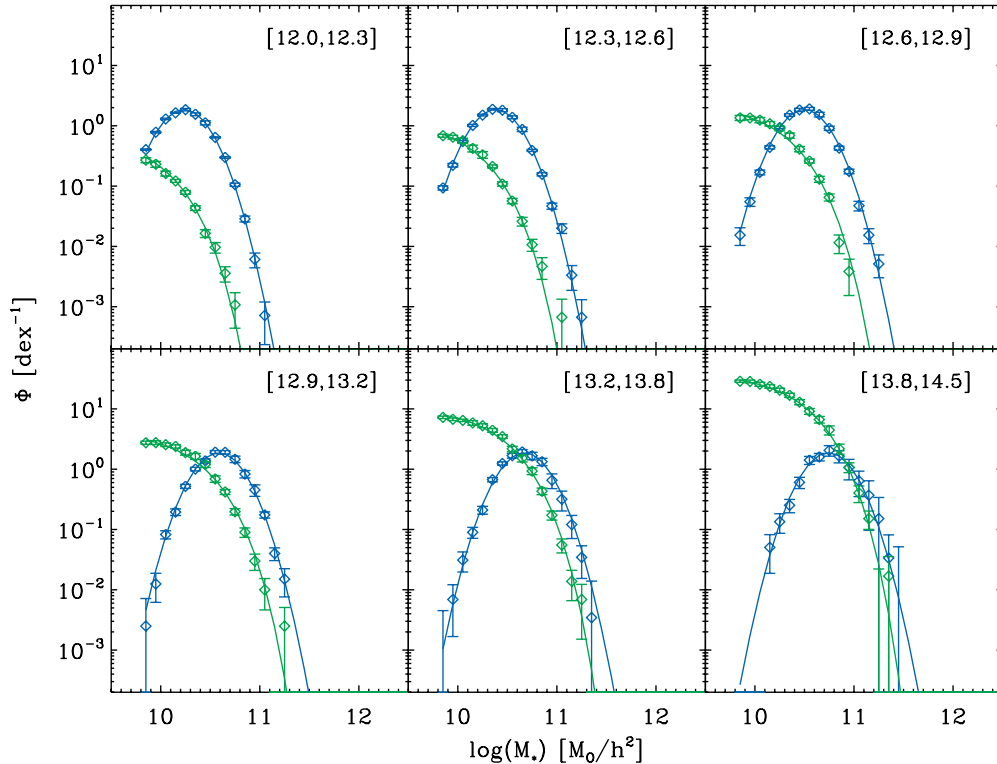


Figure 15. Comparison of the best-fit model with the DR7 SMF (points) against the full fit using host halo mass dependent parameters (lines). Host halo mass ranges are given in $\log(M_{\odot} h^{-1})$. Error bars include estimated systematic errors.

(A color version of this figure is available in the online journal.)

We fit the following functional form to the HODs drawn from these catalogs:

$$\langle N_c \rangle = \frac{1}{2} \left(1 + \operatorname{erf} \left(\frac{\ln M_{\text{host}} - \ln M_{\text{min}}}{\sigma_m} \right) \right) \quad (9)$$

$$\langle N_s \rangle = \left(\frac{M_{\text{host}}}{M_1} \right)^{\alpha_{\text{HOD}}} \exp \left(-\frac{M_{\text{cut}}}{M_{\text{host}}} \right). \quad (10)$$

M_{min} is, as described above, the cutoff in the central galaxies. The error function provides a smoothed step function that reproduces the form of the central galaxies, whose width is characterized by the parameter σ_m . The satellites are characterized by M_{cut} , the cutoff below which galaxies of the given type are not expected to have satellites, the scale M_1 at which the galaxies typically have one satellite, and α_{HOD} , the power-law slope. All mass scales increase as the stellar mass of the selected sample increases. These fits are presented in Figure 16.

Our model may be compared against the Zehavi et al. (2011) HODs fitted from clustering. An exact comparison requires the use of luminosity rather than stellar mass (see Appendices C and D for the results using r -band luminosity). Our stellar mass results show the same general trends, that is, a satellite slope of α_{HOD} consistent with one for all thresholds, decreases in all three mass scales with decreasing stellar mass, and decreasing σ_m with decreasing stellar mass. However, there are differences in detail. We find that σ_m is significantly larger, and necessarily nonzero, for all thresholds we consider. We also find a higher value of M_{min} at each threshold. This is likely due in part to the degeneracy between M_{min} and σ_m when estimating the HOD from clustering. However, it remains possible that these differences are attributable to the use of stellar mass rather than luminosity.

7. COMPARISONS WITH OTHER MEASUREMENTS

7.1. Stellar Mass Function

The precise SMF we use has a significant impact on the results and implications of our model. In other words, abundance matching is systematically dependent on the SMF used. For comparison, we consider several different SMFs from the literature, with the intent of examining how abundance matching behaves with different input. The set of SMFs we now consider is shown in Figure 17.

We give significant attention to the previous study of groups from Yang et al. (2009), of which further related details are available in Yang et al. (2005, 2007, 2008). While they use the mass-to-light ratios and $g-r$ colors based on Bell et al. (2003), the SMF from DR7 in our volume-limited catalog uses KCORRECT stellar masses from the template method of Blanton & Roweis (2007). This difference in approach introduces in effect an offset and scatter between the two definitions of stellar mass, preventing a straightforward galaxy-by-galaxy comparison. Additionally, the Bell et al. (2003) stellar masses effectively assume a Kroupa (2001) initial mass function (IMF), while we assume Chabrier (2003). The change in IMF produces an offset in stellar mass (see Figures 17 and 18).

We note that the Yang et al. (2009) results treat fiber-collided galaxies differently. In general, the Yang et al. (2009) group catalog results we consider in the next section exclude fiber-collided galaxies for which redshifts from other surveys are not available. We do not expect this to produce significant changes, as only 5% of galaxies are fiber collided in our mocks, and many of those are collided near their true redshifts.

In addition to the group catalog and associated SMF of Yang et al. (2009), we consider two additional recent measurements

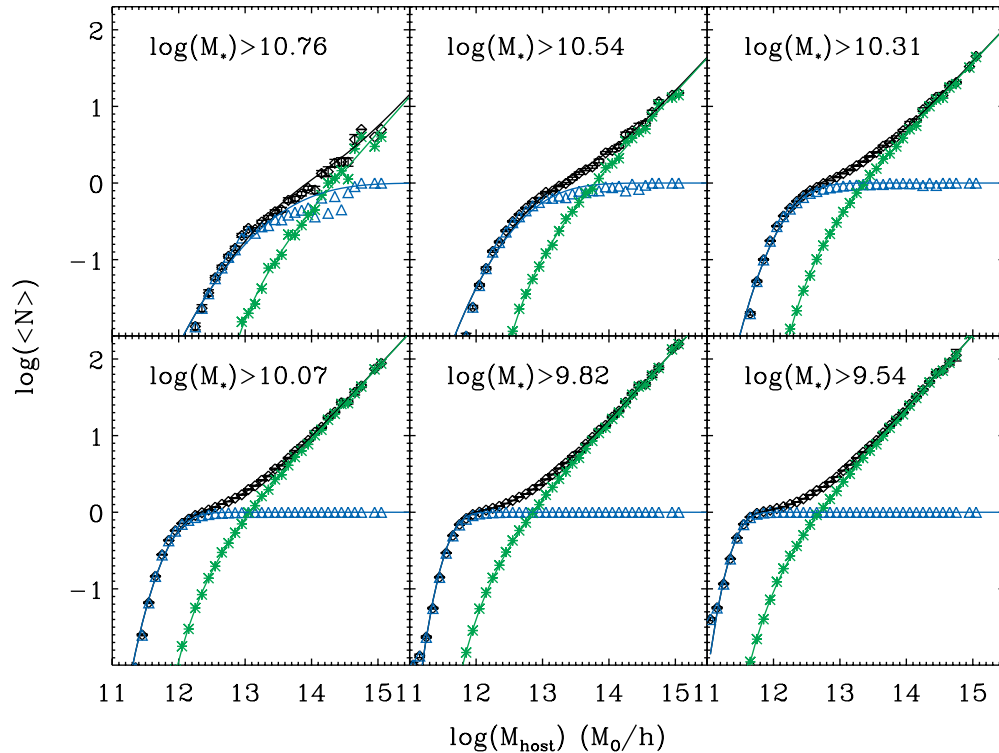


Figure 16. HOD fits for the best model. Black is the overall HOD; blue, central galaxies only; green, satellite galaxies only. Solid lines are the respective fits. Cuts in stellar mass are given in $\log(M_{\odot} h^{-2})$. Error bars have been omitted from the centrals and satellites for clarity. The HOD fit is presented in Equations (9) and (10), with parameters listed in Table 3.

(A color version of this figure is available in the online journal.)

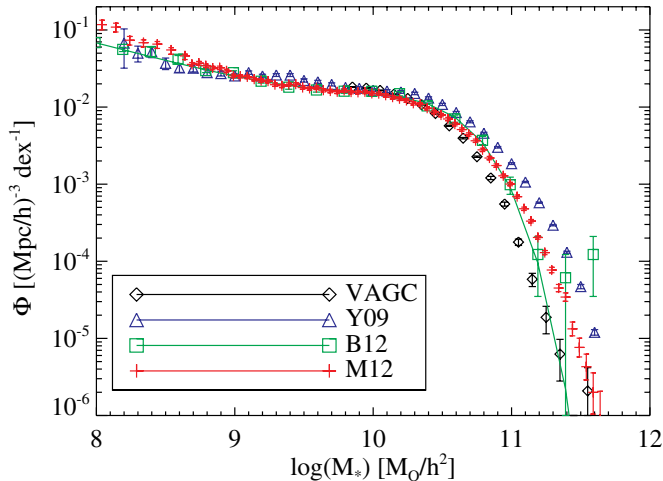


Figure 17. Four stellar mass functions from the SDSS local data. The NYU-VAGC (black) was used to fit our model parameters and tests its validity; we repeat our calculations using the others to understand the sensitivity to this global measurement. The Yang et al. (2009) stellar mass function (green) is drawn from a sample used in a previous study of the CSMF. For Baldry et al. (2012), we show both the data (square points) and their fit (line), the latter of which we use in later model tests. Finally, we also show Moustakas et al. (2013), a recent result based on SDSS combined with additional multi-wavelength data and a full Bayesian analysis of SEDs to derive stellar masses.

(A color version of this figure is available in the online journal.)

of the SMF. The first is that of Baldry et al. (2012), which applies a color-based method of estimating stellar mass which is similar in form to that of Bell et al. (2003). The data they use are drawn from the Galaxy and Mass Assembly survey at $z < 0.06$. The second is Moustakas et al. (2013), which combines SDSS data

with additional UV and IR photometry. From this data, they obtain accurate stellar masses using spectral energy distribution (SED) modeling. Their stellar population synthesis assumes a Chabrier (2003) IMF.

7.2. Intrinsic Conditional Stellar Mass Function

Two different intrinsic CSMFs can be seen directly compared in Figure 18, where the difference is the SMF input. Here, abundance matching was performed using both our VAGC derived SMF and that of Yang et al. (2009). We use the best-fit parameters found in Section 5 in both cases. It is clear that the Yang et al. (2009) CSMF generally has higher stellar mass, as expected from the change in input SMF seen in Figure 17. To more precisely quantify this difference, we fit to the intrinsic CSMF found in each of the mock catalogs produced for all four input SMFs. The fit is done as a function of host halo mass, using the parameters from Equations (3) and (4) as described in Section 6.4.

Using this overall parameterization allows a comparison between the two different SMF cases, as shown in Tables 4 and 5, by comparing just these 11 parameters for the two cases. Fits were done using the midpoint host mass value in each bin. The VAGC fit is demonstrated in Figure 15, and the fits to all four intrinsic CSMFs are shown in Figure 19. The parameters in Tables 4 and 5 demonstrate primarily the shift in stellar mass that is also visible in the figure. Note the increase in the central mass scale M_0 from our VAGC SMF to the Yang et al. (2009) result. The host halo mass scale, where the central stellar mass turns over from increasing significantly with host halo mass to a more shallow increase, is also higher in the Yang et al. (2009) case. This is most likely indicative of the change in the SMF relative to the host halo mass function, particularly

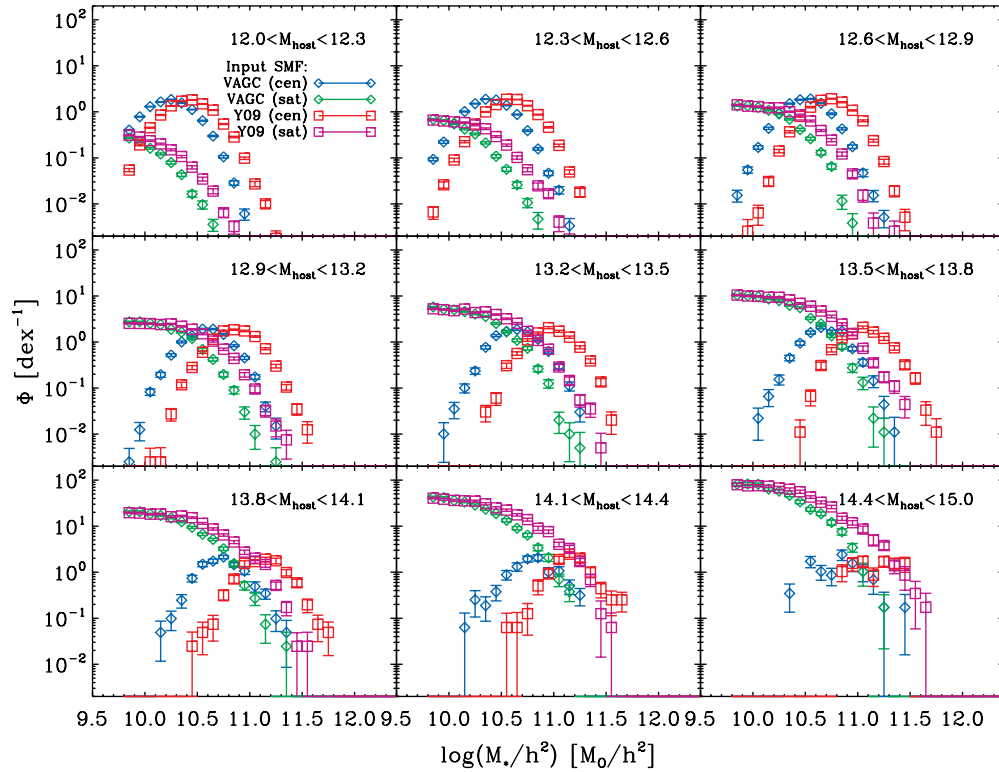


Figure 18. Comparison of the results of our best-fit abundance matching model using the SMF drawn from our volume-limited samples (centrals in blue, satellites in green) and using the SMF reported in Yang et al. (2009) (centrals in red, satellites in magenta). Ranges in host halo mass are given in $\log(M_{\odot} h^{-1})$. The primary difference between the two cases is the stellar mass definition: while we use the stellar masses from KCORRECT as described in Blanton & Roweis (2007), Yang et al. (2009) use stellar masses from Bell et al. (2003), resulting in an offset.

(A color version of this figure is available in the online journal.)

since only the high host mass slope changes significantly. The scatter in the centrals remains about the same, as expected from the fixed input model. The other two SMFs generally produce intermediate mean central stellar masses, in agreement with the different SMFs presented in Figure 17.

The VAGC version does have lower $M_{*,s}$ in general, as suggested by the slightly lower intercept value. The slightly steeper change in $M_{*,s}$ with host halo mass, as indicated by the b parameter, also pushes the characteristic stellar mass higher in the Yang et al. (2009) case. Changes in ϕ_* are somewhat more difficult to interpret, though the individual values remain similar in normalization. This is likely due to the presence of the same subhalos determining how many satellites are in each group. Most of the variation in the satellite parameters among the different SMFs stems from changes in the $M_{*,s}$ value and how it changes with M_{host} . On the other hand, ϕ_* has similar variation with group host halo mass, regardless of the SMF used.

7.3. Observed Conditional Stellar Mass Function

Direct comparisons made of the fitted CSMF results drawn from Yang et al. (2009) to our model CSMF using their SMF are shown in Figure 20. Both versions, with and without observational systematics, were done using our best-fit model (v_{peak} , scatter = 0.20 dex, $\mu_{\text{cut}} = 0.03$) applied with the SMF of Yang et al. (2009).

It is important to note the systematic differences imposed by the slightly different group finding done in these two cases. The Yang et al. (2009) results use both r -band luminosity and stellar mass information. They define their groups by requiring that at least one galaxy in each group to have $^{0.1}M_r < -19.5$.

They then use either the group total luminosity or stellar mass of all galaxies that pass that luminosity limit to assign host halo masses. They find limited differences between these using total luminosity or stellar mass. They also use the same assumption we do that the galaxy with the most stellar mass is the central galaxy.

However, the fact that their limit is a cut in luminosity rather than stellar mass significantly alters the shape of the CSMF at low host halo masses (poor groups). This effect is most clearly seen in the $12 < \log(M_{\text{host}}) < 12.3$ bin of Figure 20, which compares their results with our model, including the effects of group finding. In the Yang et al. (2009) result, their overall cut on galaxies to include is in luminosity, rather than stellar mass. This means that stellar mass of the central galaxy is not directly determining the host halo mass at low host masses, smoothing out the distribution. Aside from this difference in the low host mass bins, there is generally good agreement between our “observed” model results and these measurements.

A comparison of the intrinsic model results with these measurements is also shown in Figure 20. This demonstrates directly some of the effects of the group finding. Most obvious is the fact that the group finding reduces the width of the central distribution, as well as introducing the extra feature in low-mass host halos described above. There is also some offset in the centrals between these two cases, most likely due to the fact that the group finding assumes that the most massive galaxy in a group must be the central, pushing the observed centrals to being more massive in general. Additionally, the cutoff in the satellite distribution is much sharper after group finding. This is also due to the assignment of the most massive galaxy in the group as the central, since more massive satellites are more

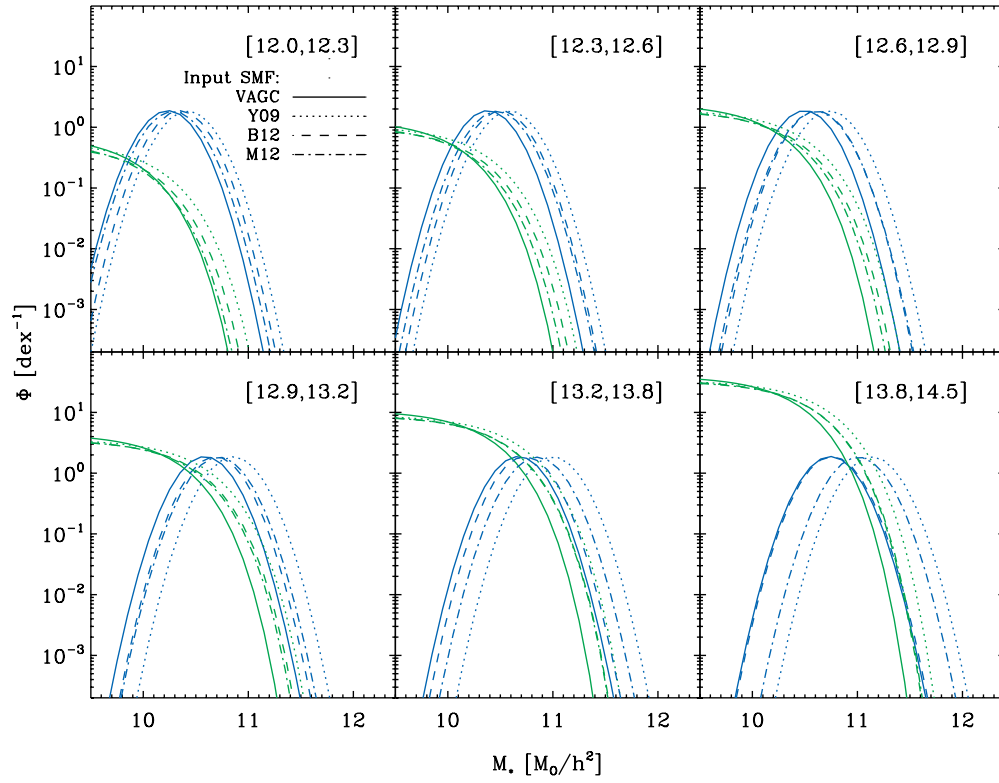


Figure 19. Comparison of fits to the intrinsic CSMF for our model using four different stellar mass functions, using the prescription discussed in Section 6.4. Blue lines indicate the central part of the CSMF, and green, the satellites. Solid lines show our main results, using the VAGC CSMF, the same as shown in Figure 15. Dotted lines show the Yang et al. (2009) SMF. Dashed lines indicate the fit to our model using Baldry et al. (2012). Dot-dashed lines show Moustakas et al. (2013). Ranges in host halo mass are given in $\log(M_\odot h^{-1})$. Note how the cutoff of the satellite stellar mass and the mean central stellar mass vary with the massive end of the SMFs shown in Figure 17.

(A color version of this figure is available in the online journal.)

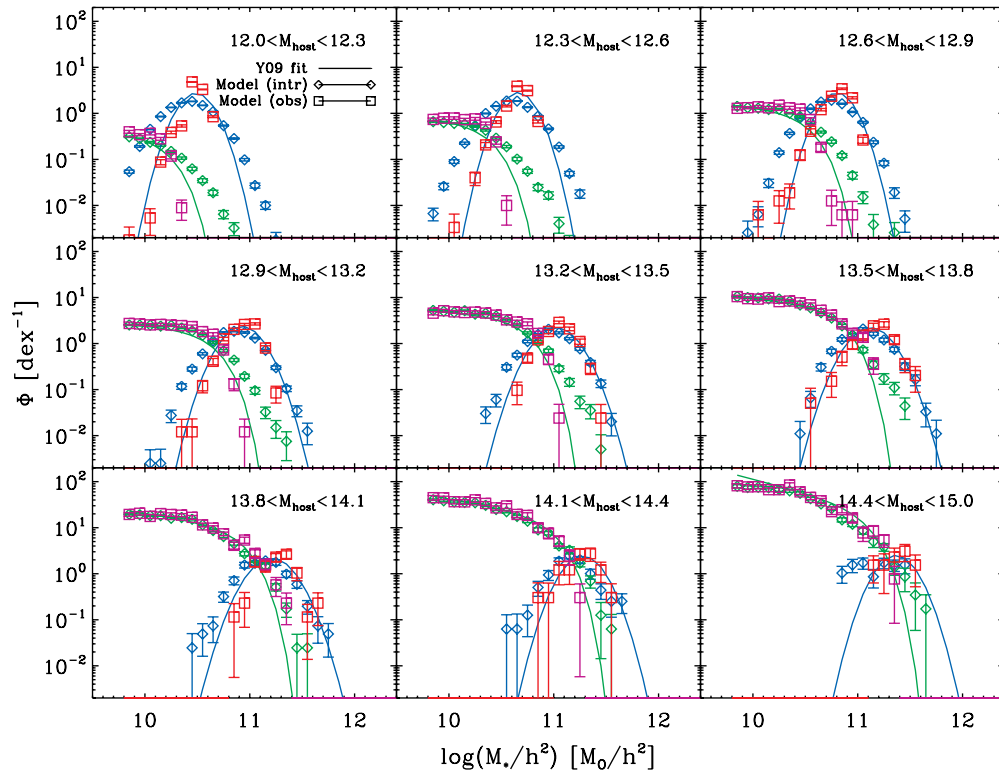


Figure 20. Results of our best-fit model using the SMF of Yang et al. (2009) before (diamonds, centrals in blue, satellites in green) and after (squares, centrals in red, satellites in magenta) the application of observational effects (group finding and fiber collisions), compared to the measurements of Yang et al. (2009) (solid lines: blue for centrals and green for satellites). Ranges in host halo mass are given in $\log(M_\odot h^{-1})$. The main difference in these two cases lies in the details of the group-finding procedure.

(A color version of this figure is available in the online journal.)

likely to be reassigned as the central. This imposes an extra cut on the satellite distribution. Therefore, it is likely that the sharp cutoff imposed on the satellite galaxies in the CSMF fits of Yang et al. (2009) is not purely physical, but convolved with the group finding.

7.4. Comparisons to Previous Work

There has been significant work in the literature regarding the question of the galaxy–halo connection. We consider a few recent examples in relation to our study.

The work of Wetzel & White (2010), using an abundance matching model based on M_{acc} , considered in detail the effect of satellite disruption in a form similar to our μ_{cut} on the clustering and satellite fraction of galaxies. They examine the disruption of satellites when the fraction $f_{\text{inf}} = M_{\text{acc}}/M_0$ of the subhalo falls below some threshold, up to $f_{\text{inf}} = 0.1$. They find that values of $f_{\text{inf}} = 0.1$ – 0.3 at $z = 0.1$ best reproduces observables, which is reassuringly similar to our preferred values for μ_{cut} . Another study was done in Watson et al. (2012) using a similar abundance matching method. They specifically addressed the stellar mass loss of satellite galaxies and the transfer of stellar mass into the intra-halo light. They considered two separate models for stellar mass loss after a subhalo was accreted. The main property of the model was gradual stellar mass loss at a rate related to the loss of dark matter after the subhalo was accreted. This is related to our consideration of the μ_{cut} parameter, though our simpler implementation assumes that the galaxy in the subhalo is rapidly destroyed after the subhalo mass falls below a threshold. They succeed in reproducing the clustering measured in Zehavi et al. (2011), including the low-luminosity thresholds. This difference may be accounted for by several differences in implementation. They use a slightly lower scatter (0.15 dex) which increases the overall clustering. They also use an analytic model for substructure (Zentner et al. 2005) rather than an N -body simulation, which permits them to track subhalos at far lower circular velocities. Nonetheless, their successful implementation is supportive of the general principle of abundance matching. Because their work shows that the satellite galaxies with the least stellar mass should also be those that are most stripped of stellar mass relative to their dark matter stripping, we suspect that the low clustering in our low stellar mass bin may be due to the loss of a few subhalos in the simulated clusters.

Another related study was done by Moster et al. (2010). They assign stellar masses using the peak subhalo mass and the present halo mass. Their work also relies on the inclusion of orphan galaxies, which may be more necessary in their work as they use a dark matter simulation with lower force resolution than Bolshoi. Rather than performing strict abundance matching using an input SMF, they assume an analytic form for the relationship between galaxy stellar mass and halo (or subhalo) mass. They then require that the model SMF is an adequate fit to that measured in SDSS (in this case, SDSS DR3). Because they use a different SMF and cosmological model, the results are slightly tricky to compare, but we note that overall their central galaxies are brighter with respect to satellites than both our model and the model of Yang et al. (2012). They successfully reproduce the two-point clustering, but do not compare with the observed CSMF, which we show provides a tighter constraint. They also note that when they use abundance matching instead of their stellar-mass–halo-mass relation, that the low halo mass end ($M_{\text{host}} < 10^{12} M_{\odot}$) of the relationship is significantly different from the power law that they assume, and add another

parameter to fit this result. The general Moster et al. (2010) form may be too restrictive at low stellar masses (see discussion in Behroozi et al. 2013a), but this halo mass is generally below what we consider.

The simple assumption in our models that scatter is constant may be modified by allowing the scatter to vary with galaxy stellar mass, halo mass, or some other halo property such as v_{max} . While the analytical model of Yang et al. (2012) incorporates these effects, it is likely that not all are necessary modifications. Another related approach was used by Neistein et al. (2011b), who use a shuffle test to determine that abundance matching may require a dependence on the host halo mass, in addition to M_{acc} , which is explored further in Neistein et al. (2011a). However, they consider only the SMF and the correlation function of galaxies in their sample, and they use only the infall mass (and host halo mass) for their abundance matching. Our analysis considers only a model with no dependence on the host halo mass. However, a more direct comparison to the results of Neistein et al. (2011a) is not immediately possible due to the difference in matching statistics (M_{acc} as opposed to our preferred v_{peak}). Regardless, degeneracies between their different models would be broken by including a comparison to the CSMF or similar group statistics.

An alternative abundance matching approach involves dividing subhalos and isolated host halos prior to abundance matching, and applying different matching functions to each. Rodríguez-Puebla et al. (2012) investigate this, decomposing the overall SMF into central and satellite components, and matching these separately to the halos and subhalos, respectively. They find that when matching against the mass of subhalos at accretion or at the present time, the satellites must have more stellar mass than would be inferred from applying the stellar-mass–halo-mass relation derived for the central galaxies. This is in general agreement with our findings as well, since the M_0 and M_{acc} direct abundance matching models have a deficit of satellites. Further, the preferred matching to v_{peak} naturally gives the subhalos of satellites higher v_{peak} than the halos of central galaxies, and thus, more stellar mass at fixed M_{peak} , as shown in Figure 2.

In contrast with our comparisons to observations, Simha et al. (2012) make a comparison between abundance matching in a purely dark matter simulation and in a dark matter simulation with the addition of gas hydrodynamics and prescriptions for star formation and feedback. The two simulations use the same initial conditions. They generally find good agreement between these cases, but there are indications of incompleteness or premature galaxy disruption at low stellar masses. However, the resolution of their dark matter simulations is not as good as that of the Bolshoi simulation that we use. Based on the results of a resolution test presented in Appendix B, we find that these discrepancies are all below the mass at which the simulation used there is able to track the full population. We thus expect that these discrepancies are primarily due to limited resolution, and not to failures of the abundance matching approach. Higher-resolution hydrodynamical simulations will be required to verify this.

One set of measurements complementary to our own are presented in More et al. (2009). Rather than using the total group stellar mass or luminosity to determine the mass of a halo, they instead use satellite kinematics to determine the mass of a halo around a central galaxy. They obtain a relationship between central galaxy luminosity and host halo mass, with a scatter of 0.16 ± 0.04 dex at fixed host halo mass. This is

somewhat low relative to our constraints for the luminosity model ($\sigma = 0.22_{-0.02}^{+0.01}$, see Appendix C for details), but our result is still within two standard deviations of theirs.

8. SUMMARY

We have used an analysis of the Bolshoi cosmological simulation to examine the correlation functions and CSMFs of several different models for the connection between galaxies and halos which are variants of the subhalo abundance matching approach. We have compared these models against data drawn from SDSS, using new measurements of the two-point correlation function as a function of stellar mass and the CSMF in groups. All CSMF comparisons between models and data are done in “observed space,” after applying group finding and fiber collisions to our models. Our study is the first to combine this set of measurements in a fully self-consistent way to test a model which assigns all galaxies to resolved subhalos in a simulation. From these results, we have reached the following conclusions.

1. An examination of the correlation function shows that most of the halo mass properties used as proxies for stellar mass that we considered cannot reproduce the data regardless of the parameters used. This includes abundance matching models where the halo property used is M_0 , M_{acc} , M_{peak} , $M_{0,\text{peak}}$, v_{max} , and v_{acc} . Each of these models is insufficiently clustered even in cases with no scatter and $\mu_{\text{cut}} = 0$. Because nonzero scatter and μ_{cut} only reduce galaxy clustering, we exclude those models. The only exceptions are v_{peak} and $v_{0,\text{peak}}$. This exclusion applies only to this particular family of models, and cannot be applied to models with significantly different methodology, such as those which incorporate orphan galaxies.
2. Our best-fit model uses v_{peak} , with $\mu_{\text{cut}} = 0.03$ and scatter of 0.20 dex. This scatter is effectively the combination of intrinsic scatter in stellar mass and scatter from the measurements because we do not distinguish between them. This model provides a good fit to the combined constraints of the clustering for galaxies with $\log(M_*) > 10.2$, the mean and dispersion of the central galaxies in bins of host mass (in the CSMF), and the satellite distribution in the CSMF, both for galaxies brighter than $\log(M_*) > 9.8$.
3. The $v_{0,\text{peak}}$ model provides significantly poorer fits to the data overall than v_{peak} . It can marginally fit the clustering data alone, but cannot fit the satellite CSMF and is strongly ruled out by the combined data. The increased stellar mass of satellites relative to central galaxies forces the mean stellar mass of the central CSMF slightly low. The high μ_{cut} needed to match the clustering also reduces the satellite fraction at low stellar masses too much to reproduce the satellite distribution.
4. The scatter is most strongly constrained by the width and mean of the distribution of galaxies in groups, both centrals and satellites. Thus, the central CSMF provides the sharpest limit. This strongly excludes zero (or very low) scatter, and scatter above 0.25 dex. We estimate scatter of $\sigma = 0.20 \pm 0.03$ dex in stellar mass at fixed v_{peak} .
5. We explicitly test the mass dependence of the scatter value, using the CSMF in bins of total stellar mass, and find that it is consistent with being constant for the galaxies living in halos from 10^{12} to $10^{14} M_{\odot} h^{-1}$. Changes by more than 0.1 dex over this range are ruled out.
6. The value of μ_{cut} is only weakly constrained for the v_{peak} model. A value of zero is weakly disfavored by the

CSMF; the correlation function disfavors values above 0.08. Marginalizing over scatter results in a 1σ upper limit of $\mu_{\text{cut}} < 0.07$.

7. The projected correlation function using this v_{peak} model is low for the $\log(M_*) > 9.8$ threshold at small scales. This may be due to loss of a few low stellar mass satellites, suggesting that even the Bolshoi simulation may be inadequate at tracking subhalos at these masses, and that properly reproducing the galaxy distribution may require the inclusion of orphan galaxies. Another possibility is that our model is too simple; loss of substructures is degenerate with a mass dependence in the μ_{cut} parameter, which could have similar impact on the satellite fraction. Alternatively, the discrepancy may be due to inadequately modeling the observational effects on galaxies at these stellar masses when calculating the correlation function.
8. The fact that only the v_{peak} model is capable of reproducing the data indicates that satellites typically have more stellar mass than central galaxies for a given (sub)halo mass such as M_{peak} . This is in general agreement with other recent models, such as those of Guo et al. (2011), Neistein et al. (2011a), Rodríguez-Puebla et al. (2012).

The subhalo abundance matching model presented here is capable of reproducing all the trends expected from the measurements we consider, particularly the projected correlation function and the CSMF, when specific assumptions are made about the parameter on which to abundance match, the value of the scatter, and the halo stripping required to remove a galaxy from the sample. This is true even for the simple assumptions used—fixed scatter in stellar mass, and no dependence on when v_{max} is assigned to satellites.

Using this model, the data are only reproduced within the very small statistical errors for $\log(M_*) \gtrsim 10.0$. Below this stellar mass there appears to be slightly fewer satellites in the model. Possible explanations include observational systematics, required variation in the mass threshold for destroying satellites, or the need for inclusion of subhalos below the resolution limit of the simulation. In the context of the current approach, we cannot distinguish between these. We intend to revisit this issue in the future using a combination of data that is complete to lower stellar masses and higher-resolution simulations.

In this work, we have only tested a single cosmology. The fact that the CSMF and correlation function can be well reproduced suggests that our chosen cosmology is very close to the correct model. This is further supported by the fact that we well reproduce other measures not directly used to constrain the model parameters, in particular, the group total SMF, which depends on the halo mass function (and thus on σ_8) for a given clustering strength.

We also focus primarily on the results using the ROCKSTAR halo finder. Using the BDM halo finder (Klypin et al. 1999) does not produce significantly different results. However, there are slightly fewer galaxies in the model applied to the BDM halos than in the ROCKSTAR case, most likely because ROCKSTAR finds more substructure, particularly near the centers of halos.

This same analysis may be applied to samples based on luminosity, rather than stellar mass. While the framework remains unchanged, the results may be slightly different, as a galaxy remaining at fixed stellar mass after being accreted will dim in luminosity as its stars age. This will reduce the luminosity of satellites compared to centrals, unlike stellar mass. At a given number density of objects, this will mean that the satellite fraction at the specified luminosity should

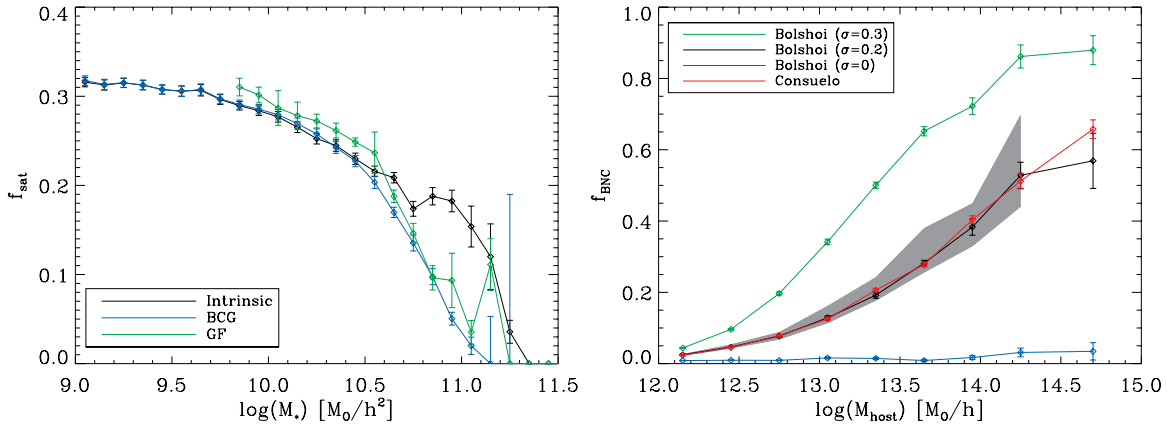


Figure 21. Left: effect of group finding on the satellite fraction. The intrinsic satellite fraction in the model (black) is significantly higher than when reassigning the brightest cluster galaxy as the central (blue) in galaxies with high stellar masses. This is because the nonzero scatter allows a significant number of true satellites to be scattered up in stellar mass, increasing the satellite fraction of massive galaxies. This effect increases with scatter; in a zero-scatter model, the change is negligible. This is also the primary difference between the intrinsic satellite fraction and that obtained via the group finder (green). All lines are for the $v_{\text{peak}}, \mu_{\text{cut}} = 0$, scatter = 0.20 dex model. Right: fraction of central galaxies where at least one satellite in the same halo has higher stellar mass. The result is shown on the mocks for two different simulation, the Bolshoi simulation (black) and the Consuelo simulation (red) which is lower resolution. These both use a model with stellar mass, $v_{\text{peak}}, \mu_{\text{cut}} = 0.03$, and scatter of 0.20 dex. Error bars show statistical jackknife errors. The gray band gives the resulting range in the f_{BNC} fraction given the 1σ range in scatter for the fitted Bolshoi model. This probability is also shown for two other values of scatter (0.30 dex and zero) in Bolshoi, which are ruled out by the data.

(A color version of this figure is available in the online journal.)

be slightly lower than the satellite fraction at the equivalent stellar mass. A demonstration of this difference may be seen in Appendix C. While the scatter estimated by this method is similar (~ 0.20 dex), it produces a significantly higher value of $\mu_{\text{cut}} = 0.13$ (versus 0.03 for stellar mass), and a resulting lower satellite fraction.

In the local universe, further improvements may be possible by including additional measurements in a self-consistent approach, including the velocity dispersion of galaxies in groups, galaxy–galaxy lensing, the Tully–Fisher relation (as was done by Trujillo-Gomez et al. 2011), and the properties of bright galaxies (e.g., Hearin et al. 2013). Additional constraints on the bright sample are also possible using larger volume. Future work may determine how well this model performs at higher redshift. At present, the study is only possible at this level of detail in the local universe, but larger spectroscopic samples are becoming available at higher redshift. An extension of our modeling approach to photometric data will be important to take account of the large amount of information from upcoming imaging surveys.

The detailed understanding of the galaxy–halo connection we have presented here has implications for a wide range of areas in galaxy formation and cosmology. We expect the constraints provided on the intrinsic CLF will be very helpful in constraining semi-analytic galaxy formation models and hydrodynamical simulations. These constraints can also be used to implement CLF- or CSMF-based modeling on larger, lower-resolution simulations. This will be important for accurately modeling the distribution of dimmer galaxies and forecasting how well future imaging surveys, such as the Dark Energy Survey and the Large Synoptic Survey Telescope, can constrain cosmological parameters. Uncertainty in the connection between galaxies and halos is an important systematic in several methods to constrain cosmological parameters. Examples include the precise determination of galaxy bias required for clustering and lensing constraints, understanding the galaxy content of clusters for cluster cosmology (Roze et al. 2010; Tinker et al. 2012), and modeling the mass along the line of sight to strong lensing time delays (Suyu et al. 2010). The pre-

cise constraints we now provide in the nearby universe are a step toward minimizing these systematics and achieving the precision required for next generation cosmological measurements.

R.M.R. is supported by a Stanford Graduate Fellowship. This work was additionally supported by the U.S. Department of Energy under contract number DE-AC02-76SF00515, and a Terman Fellowship to R.W. at Stanford University. This research was also supported in part by the National Science Foundation under grant No. NSF PHY11-25915, through a grant to KITP during the workshop “First Galaxies and Faint Dwarfs.” This work used computational resources at SLAC.

We thank Yu Lu, Michael Busha, Frank van den Bosch, Andrew Zentner, Anatoly Klypin, and Cameron McBride for useful discussions, and Andrew Wetzel, Douglas Watson, Matt George, and Surhud More for comments on a draft. We thank the anonymous referee for several suggestions that improved the presentation of this work. We are grateful to Anatoly Klypin and Joel Primack for providing access to the Bolshoi simulation, which was run on the NASA Ames machine Pleiades. This work also uses data from the LasDamas simulations. These were run using computational resources at Teragrid/XSEDE and at SLAC. Further information is available at <http://lss.phy.vanderbilt.edu/lasdamas/>. We are grateful to our LasDamas collaborators, and especially Michael Busha and Cameron McBride, who ran the Consuelo and Esmerelda simulations used here. We also thank Cameron McBride for providing a copy of the program for making mock fiber collisions and John Moustakas for providing his derived SDSS SMF prior to publication.

Funding for the Sloan Digital Sky Survey (SDSS) has been provided by the Alfred P. Sloan Foundation, the Participating Institutions, the National Aeronautics and Space Administration, the National Science Foundation, the U.S. Department of Energy, the Japanese Monbukagakusho, and the Max Planck Society. The SDSS Web site is <http://www.sdss.org/>. The SDSS is managed by the Astrophysical Research Consortium (ARC) for the Participating Institutions. The Participating Institutions are The University of Chicago, Fermilab, the Institute for

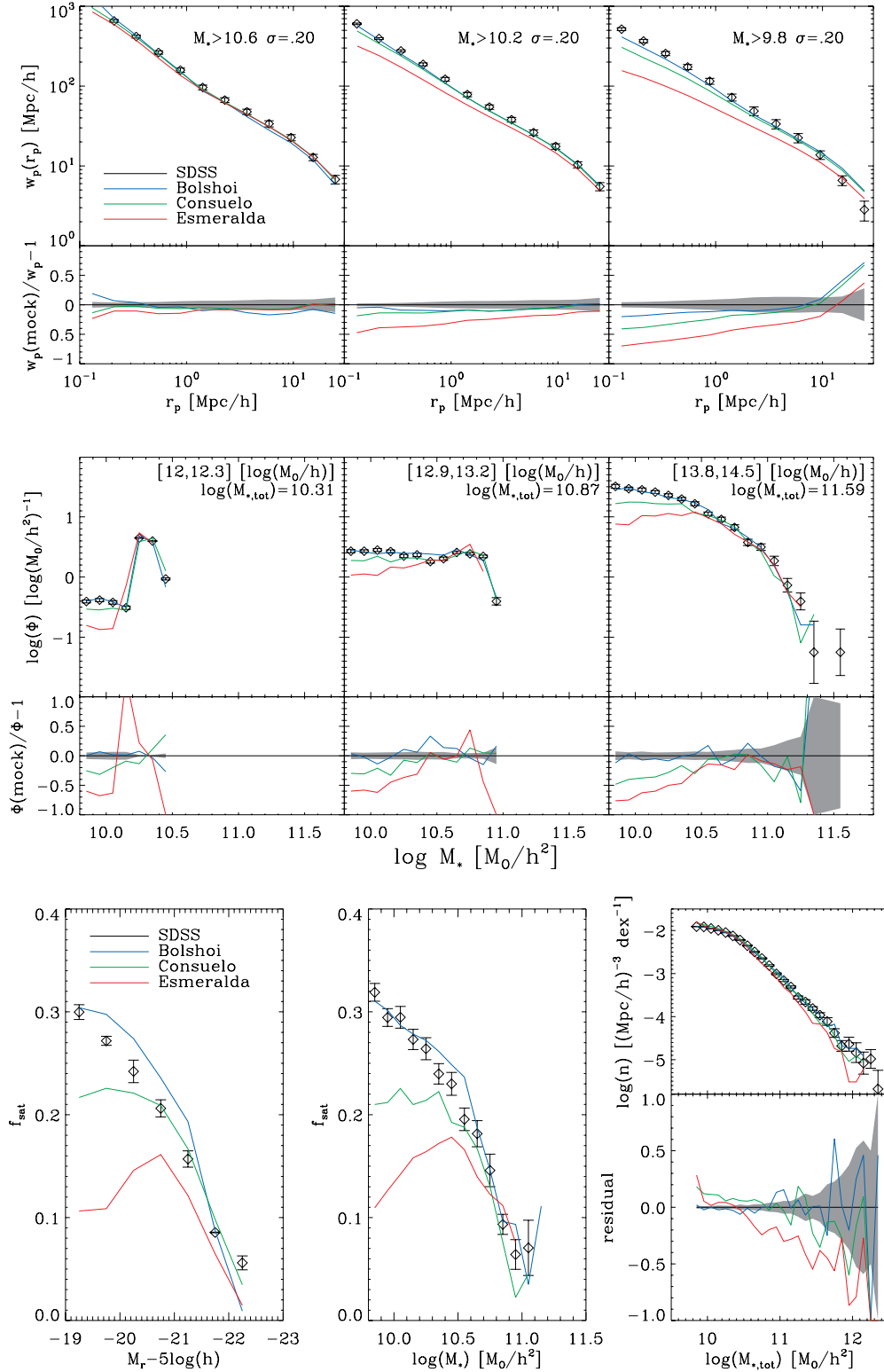


Figure 22. Impact of simulation resolution on statistics of resolved subhalos. Figure shows the v_{peak} model with $\mu_{\text{cut}} = 0$ and $\sigma = 0.2$, applied to the Bolshoi (blue), Consuelo (green), and Esmeralda (red) simulations, with the measured values from the SDSS DR7 VAGC (black) shown for comparison. The inability of lower-resolution simulations to resolve all satellite halos results in a deficit of satellites and a drop in the small-scale clustering. Top: correlation functions. Center: conditional stellar mass functions. Total stellar mass is given in $\log(M_{\odot} h^{-2})$. Bottom left: satellite fraction for the luminosity model with these parameters. Bottom center: satellite fraction in the stellar mass model. Bottom right: group total stellar mass function. Based on the results from the satellite fraction, the Bolshoi, Consuelo, and Esmeralda simulations are roughly complete for satellite galaxies at stellar masses of $\log(M_{*}/(M_{\odot} h^{-2})) = 10.0, 10.5,$ and 10.8 , respectively, or at luminosities of $M_r - 5 \log(h) < -19.5, -20.5,$ and -21.5 .

(A color version of this figure is available in the online journal.)

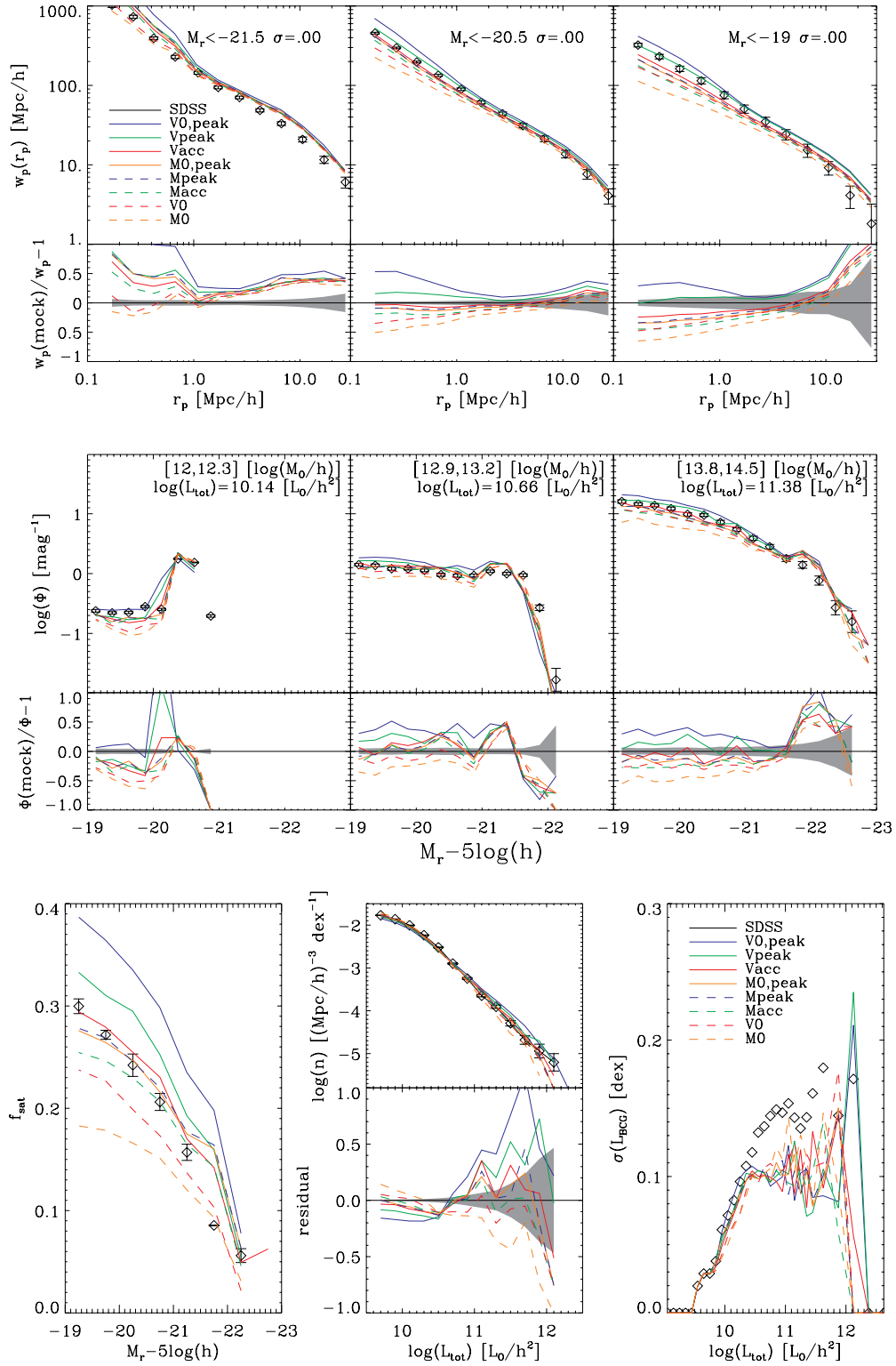


Figure 23. Abundance matching results matching galaxy luminosity to different halo properties. All shown here have zero scatter and $\mu_{\text{cut}} = 0$. Top: projected two-point correlation function. Labels denote the luminosity thresholds. Changes in model here are generally most noticeable in the one-halo term. Because increases in scatter or μ_{cut} can only decrease the clustering, it follows that any model which falls significantly below the measured clustering (black) must be excluded. Center: conditional luminosity function (CLF). Labels indicate the range in $\log(M_{\text{vir}})$ for each plot. Nonzero scatter broadens this part of the distribution. Bottom left: satellite fraction as a function of luminosity. As should be expected, models with higher satellite fraction correlate with stronger one-halo clustering and more satellites in the CLF. Bottom center: group luminosity function. Bottom right: standard deviation (scatter) in stellar mass of central as a function of total group stellar mass. Error bars on the models are suppressed for clarity.

(A color version of this figure is available in the online journal.)

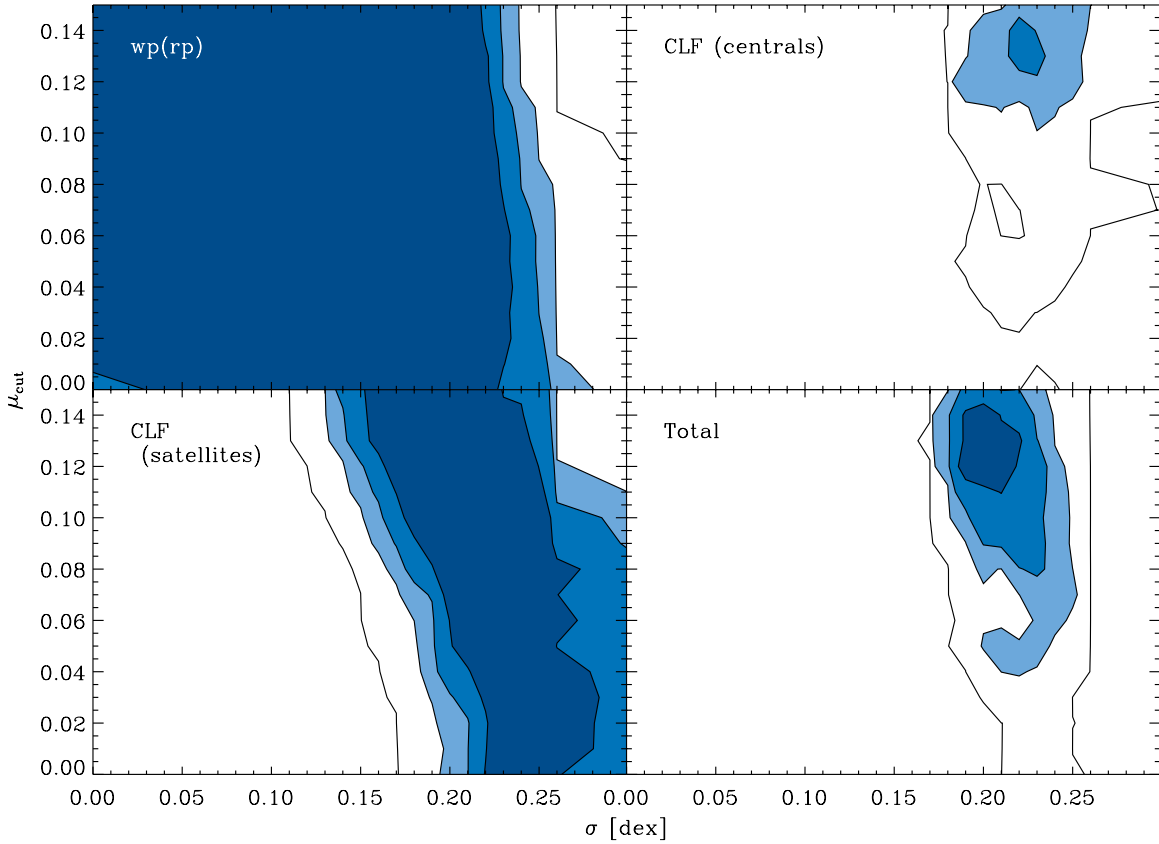


Figure 24. Constraint on the scatter and μ_{cut} when using v_{peak} . Levels give $P(>\chi^2)$, corresponding to 1σ , 2σ , 3σ , and 5σ contours. Top left: constraint from clustering only. Top right: constraint from central part of CLF only. Lower left: constraint from satellite part of CLF only. Lower right: constraint from all measures combined. (A color version of this figure is available in the online journal.)

Advanced Study, the Japan Participation Group, The Johns Hopkins University, Los Alamos National Laboratory, the Max-Planck-Institute for Astronomy (MPIA), the Max-Planck-Institute for Astrophysics (MPA), New Mexico State University, University of Pittsburgh, Princeton University, the United States Naval Observatory, and the University of Washington.

APPENDIX A

EFFECTS OF THE GROUP FINDER

The group finder itself has a significant impact on our various measurements. As discussed in the main text, the two primary systematic effects of the group finder are the artificial reduction of scatter in central galaxy stellar mass for low halo masses, and the assumption that the most massive galaxy in a group must be the central. A clear demonstration of this may be seen in Figure 21. Here, we show the difference in the model satellite fraction between using the intrinsic central galaxies, and assuming that the most massive galaxy is the central, both using the intrinsic group assignment. As expected, this significantly reduces the satellite fraction of massive galaxies, since in large clusters it is not unlikely for at least one satellite to be more assigned a higher stellar mass than the central. (This can be seen in the intrinsic CSMF in Figure 12.) This is the primary reason for the difference in satellite fraction between the intrinsic satellite fraction and that obtained from the group finder. Furthermore, this effect becomes stronger in models with increased scatter, because non-central galaxies are more likely to be scattered up in stellar mass than the intrinsic central, and is almost negligible in models with zero scatter.

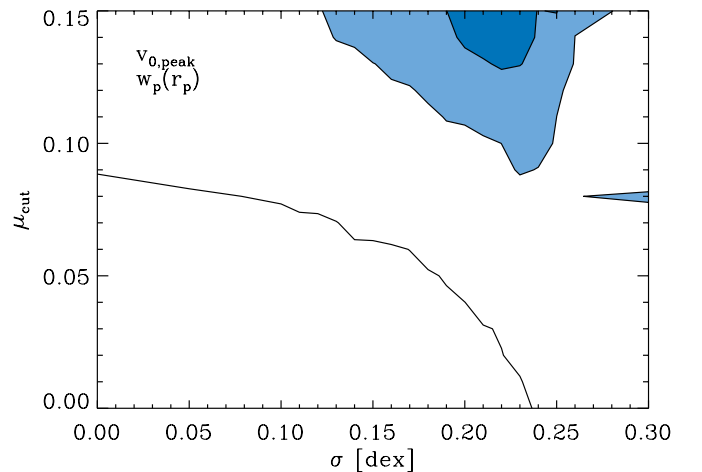


Figure 25. Same as Figure 24, but using $v_{0,\text{peak}}$. Constraints on the scatter and μ_{cut} . Levels give $P(>\chi^2)$, corresponding to 1σ , 2σ , 3σ , and 5σ contours, though here only the upper right corner with the 5σ contour appears. The central and satellite CLF, and overall fit are everywhere more than 5σ deviations, and therefore omitted.

(A color version of this figure is available in the online journal.)

The fraction of central galaxies that do not have the most stellar mass (or are not the brightest) increases with host halo mass, as can be seen in the right-hand plot of Figure 21. It also increases with intrinsic scatter, but is not strongly dependent on the resolution of the dark matter simulation. The values we find for moderate scatter are in general agreement with the

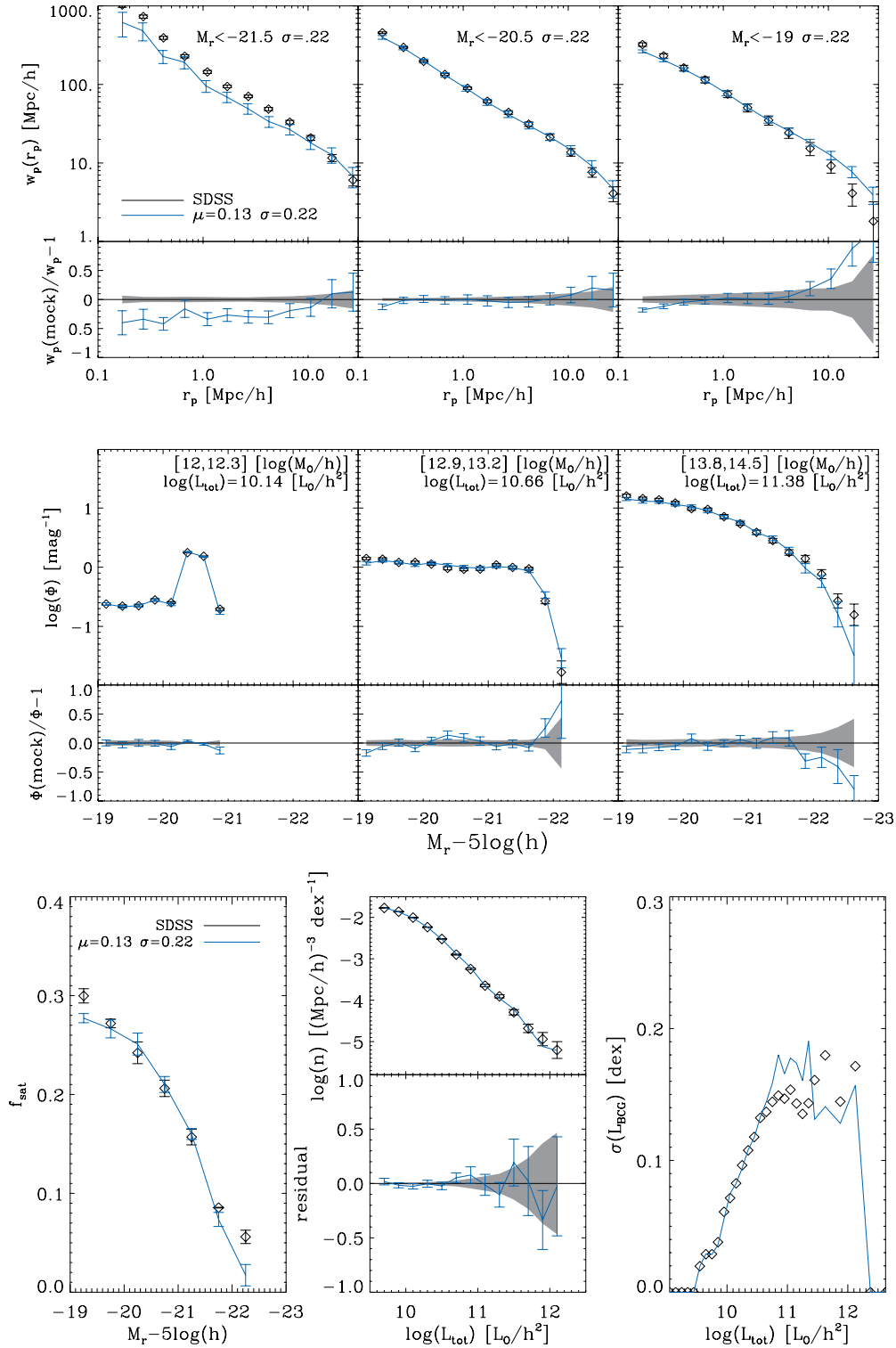


Figure 26. Best-fit model when using v_{peak} , with $\mu_{\text{cut}} = 0.13$, scatter = 0.22 dex. Plots are the same as described in Figure 23. The low clustering of the $M_r < -21.5$ threshold is likely due to the high μ_{cut} value, but this does not have a large impact on the fit due to the large errors and correlations between data points.

(A color version of this figure is available in the online journal.)

study of Skibba et al. (2011). The recent weak lensing study of George et al. (2012) tests multiple different center definitions for groups with a range in M_{host} of 10^{13} – $10^{14} M_{\odot}$. They find that $\sim 20\%$ – 30% of these groups have “ambiguous” centers, where multiple center definitions are in significant disagreement. This is also in good agreement with the fractions we measure in Figure 21.

This effect of group finding can also be seen in a comparison between the intrinsic CSMF (Figure 12) and that obtained after the use of the group finder (Figure 8). Note that although the distribution of galaxies in massive halos is not strongly changed, the central distribution in the low-mass halos sharpens considerably after group finding, lowering the inferred scatter due to correlations between central properties and group properties.

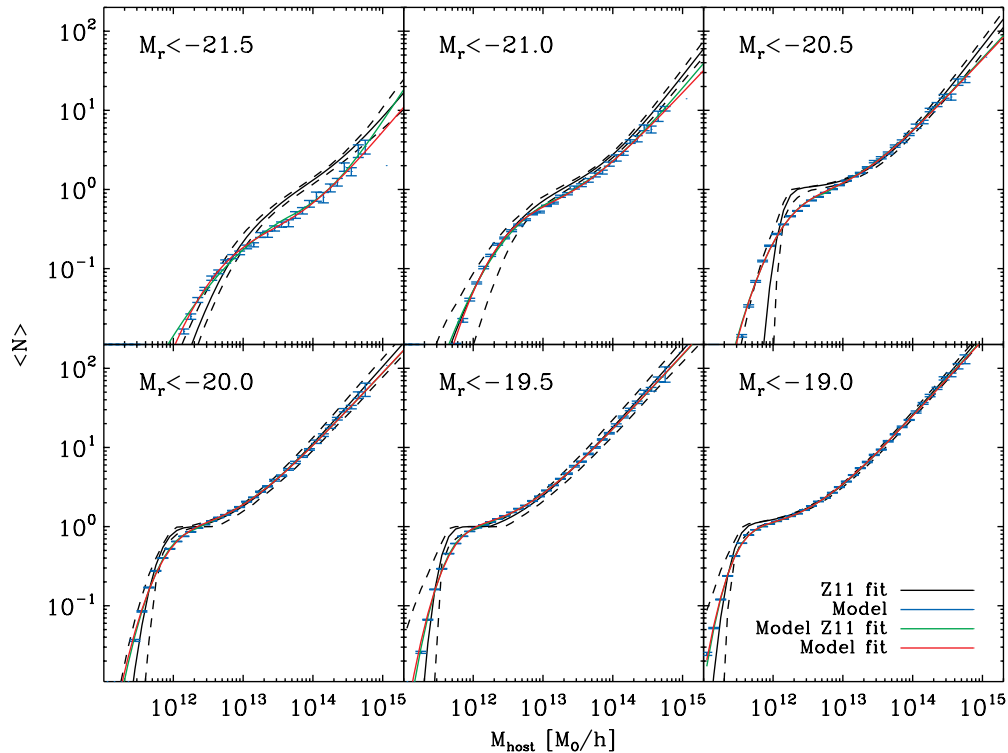


Figure 27. Comparison of the best-fit model (abundance matched to luminosity) with Zehavi et al. (2011) HOD derived from a fit to SDSS clustering measurements. Solid black lines show the Zehavi et al. (2011) HOD, with dashed lines showing the 1σ bounds based on the parameters they provide for their fit, assuming no correlation among parameters. Blue error bars are the model results. The green line is the fit to the model results using the Zehavi et al. (2011) parameterization from Equation (D1), while the red line shows our parameterization from Equations (9) and (10), and modified as described in Appendix C. The primary difference between the two lies in the location and width of the central host mass cutoff, which are somewhat degenerate when fitting to clustering measurements. While this form provides a good fit to the overall HOD, it does not well describe the central and satellite parts of the HOD separately.

(A color version of this figure is available in the online journal.)

APPENDIX B RESOLUTION REQUIREMENTS

The use of a high-resolution simulation such as Bolshoi is essential to this work. A simulation with more massive particles or a larger softening length would not be able to resolve as many subhalos, particularly those near the center of massive clusters (see Behroozi et al. 2013b and Onions et al. 2012 for related subhalo information, and Wu et al. 2013 for a more detailed discussion) which tend to be victims of “overmerging” or otherwise become prematurely disrupted. Figure 22 shows the difference between using Bolshoi, and the Consuelo and Esmeralda simulations from the LasDamas suite (C. McBride et al. 2009). Consuelo (see also Behroozi et al. 2013b; Leauthaud et al. 2011) uses 1400^3 particles in a volume of $(420 h^{-1} \text{ Mpc})^3$ (with a particle mass of 1.9×10^9), while Esmeralda has 1250^3 particles in $(640 h^{-1} \text{ Mpc})^3$ (with a particle mass of 9.3×10^9). Bolshoi, Consuelo, and Esmeralda have (physical) force resolution of 1, 8, and 15 kpc h^{-1} , respectively.

The same abundance matching model was applied to all three simulations. As can be seen in the figure, the model applied to Consuelo (with the same parameters) has a significant deficit of satellites with $M_* > 10.5$, while the loss of satellites in Esmeralda is even more severe. Because smaller subhalos are more easily disrupted, there are fewer of them. Thus, for a selection at a fixed stellar mass to have the appropriate number density from abundance matching, a mixture of smaller halos (and sometimes subhalos) will be given a greater stellar mass than they would be assigned if the prematurely disrupted

subhalos had not been lost. Most of these halos will be isolated halos, reducing the satellite fraction. This also reduces the clustering, particularly at the small scales where satellites contribute strongly.

Furthermore, this effect is worsened when using a property other than v_{max} or M_0 for abundance matching. In particular, when using v_{peak} as the abundance matching parameter as shown in the figure, there will be numerous relatively smaller subhalos at the present time which had a much higher v_{max} in the past, but are now lost to the simulation. The additional force resolution of the Bolshoi simulation does a better job of capturing these satellites that have experienced significant stripping of their dark matter mass, allowing them to be tracked substantially longer than they can be tracked in the lower-resolution Consuelo or Esmeralda simulations.

APPENDIX C USING LUMINOSITY

We have repeated the entire study using luminosity in the SDSS r band. The global luminosity function from the SDSS (Blanton et al. 2003a), while having more information on dimmer galaxies, is not precisely the same as the luminosity function in our sample. Therefore, for consistency with the group catalog, we use the luminosity function of galaxies in the corresponding volume-limited sample to perform the abundance matching, as was done when using stellar mass. For comparisons of the two-point correlation function, we use the measurements of Zehavi et al. (2011) defined with luminosity thresholds.

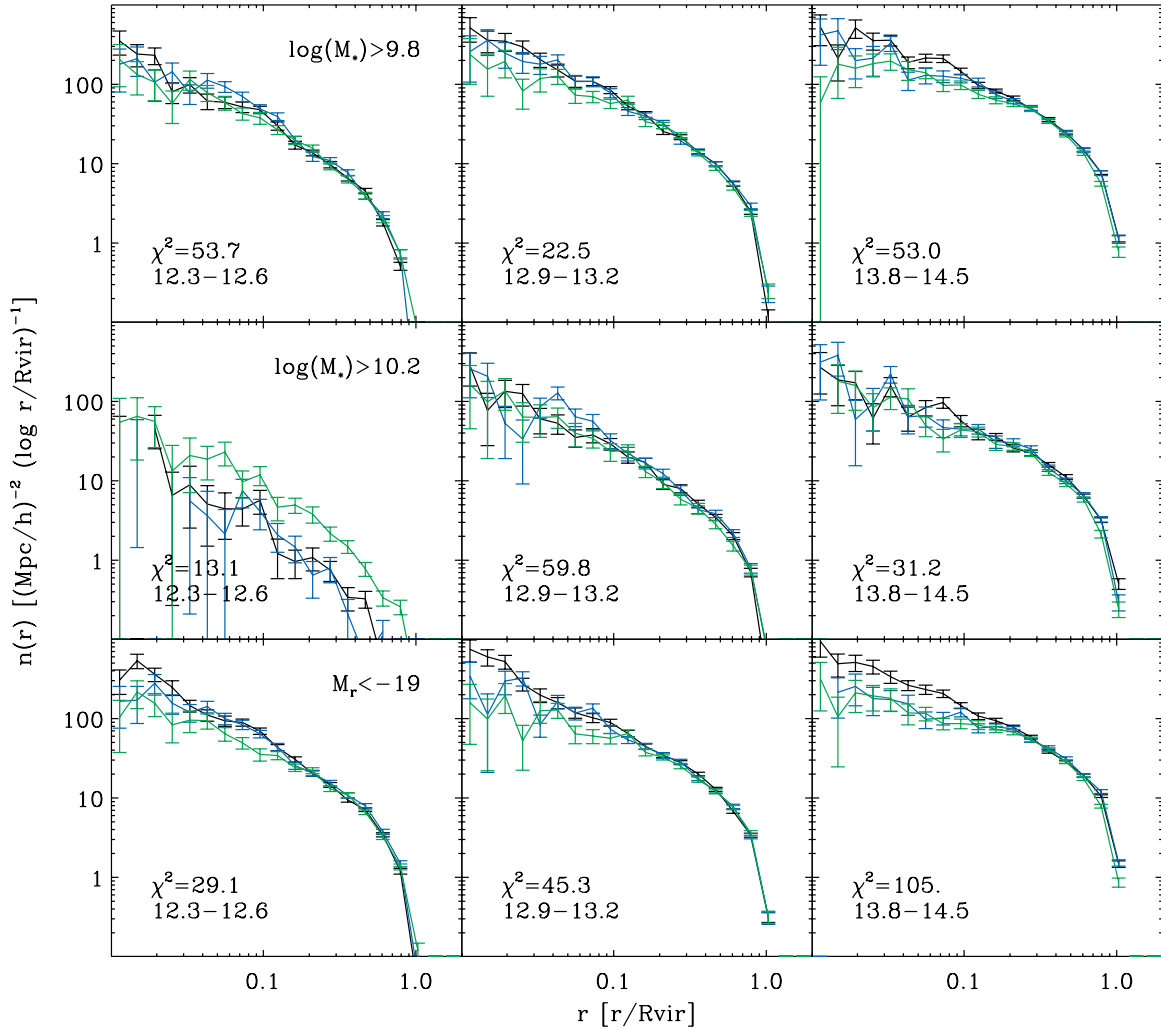


Figure 28. Projected radial profiles of galaxies in halos, for different cuts in stellar mass or luminosity. Top: radial profiles for stellar masses with $\log(M_*) > 9.8$. Center: stellar masses with $\log(M_*) > 10.2$. Bottom: luminosity cut at $M_r < -19$. In all plots, black is SDSS; blue is the best-fit model as it would be observed, which is v_{peak} , $\mu_{\text{cut}} = 0.03$, scatter = 0.20 dex for stellar mass, and $\mu_{\text{cut}} = 0.13$ and scatter = 0.22 dex for luminosity. Green is the intrinsic projected radial profile (without group finding). χ^2 values indicate the quality of the fit at $r/R_{\text{vir}} > 0.1$ (nine data points). While the fit in that range is quite good, it tends to fail at smaller radii, particularly for the more massive groups.

(A color version of this figure is available in the online journal.)

The same general trends apply for luminosity as for stellar mass, with a few complications. First, while we use the same volume-limited sample as for the stellar mass-based comparison, the luminosity completeness limit is at $M_r < -19$. We therefore have more galaxies present in a sample of the same volume in the luminosity sample. Additionally, here we correct for changes in inferred absolute magnitude due to changes in inferred redshift due to fiber collisions, using the k -corrections to the r band from Blanton & Roweis (2007).

Constraints are calculated including all correlations functions shown, and the central and satellite parts of the CLF. The best-fit results are again for v_{peak} , but this time with $\mu_{\text{cut}} = 0.12$ and scatter of 0.21 dex. (When not using the local averaging procedure, the best fit lies at $\mu_{\text{cut}} = 0.13$ and scatter of 0.22 dex.) Marginalizing over μ_{cut} , we obtain limits of $\sigma = 0.210^{+0.01}_{-0.02}$ dex (68%) and $\sigma = 0.21^{+0.02}_{-0.03}$ dex (95%). Marginalizing over scatter, the μ_{cut} limits are $\mu_{\text{cut}} = 0.12^{+0.02}_{-0.01}$ (68%) and $\mu_{\text{cut}} > 0.09$ (95% limit).

While the scatter agrees with our results for stellar mass, the μ_{cut} value is significantly higher. This is favored by the

parts of the CLF, which contribute most of the χ^2 , but not by the clustering alone, as can be seen with the low clustering in the brightest sample. The v_{peak} model fits the satellite CLF somewhat well, but the group LF is low for small groups, and there is some offset in the central part of the CLF.

It remains true that $v_{0,\text{peak}}$ fits badly on all counts, being overclustered and having too many satellite galaxies. (See Figure 23 for the comparison of different matching parameters with luminosity.) Neither v_{peak} or $v_{0,\text{peak}}$ provides a good fit to the central part of the CLF, due primarily to an offset in the mean. Even the best-fit v_{peak} produces centrals that are too dim in low halo masses, and $v_{0,\text{peak}}$ centrals are too dim at low masses and somewhat too bright at higher halo masses. The constraints are shown in Figures 24 and 25, with the best-fit results in Figure 26. The CLF fit parameters are given in Table 6, and the HOD fit is given in Table 7. Note that the C_{cen} value is an additional multiplicative factor applied to the central HOD, to account for the number of centrals not reaching unity for some luminosity thresholds.

Table 6
Intrinsic CLF Luminosity Fit Parameters for Best-fit Model

M_{host} ($\log(M_{\text{vir}})$)	$\log(L_c)$ ($\log(L_\odot h^{-2})$)	σ_c ($\log(L_\odot h^{-2})$)	ϕ_* ($\log(L_\odot h^{-2})^{-1}$)	α	$\log(L_*)$ ($\log(L_\odot h^{-2})$)	No. of Hosts
12.0–12.3	10.024 ± 0.001	0.2338 ± 0.0008	1.16 ± 0.06	−0.93 ± 0.08	9.77 ± 0.02	27948
12.3–12.6	10.150 ± 0.002	0.227 ± 0.001	2.34 ± 0.08	−0.684 ± 0.060	9.842 ± 0.018	14983
12.6–12.9	10.238 ± 0.003	0.224 ± 0.001	4.36 ± 0.16	−0.738 ± 0.050	9.923 ± 0.016	7814
12.9–13.2	10.284 ± 0.004	0.228 ± 0.002	7.54 ± 0.31	−0.820 ± 0.046	10.008 ± 0.017	4000
13.2–13.8	10.332 ± 0.004	0.230 ± 0.002	18.0 ± 0.6	−0.893 ± 0.033	10.054 ± 0.013	2896
13.8–14.5	10.381 ± 0.009	0.217 ± 0.004	66.2 ± 3.1	−0.995 ± 0.042	10.091 ± 0.015	595

Table 7
Intrinsic HOD Luminosity Fit Parameters for Best-fit Model

M_r Threshold	M_{min} ($\log(M_\odot h^{-1})$)	σ_m ($\log(M_\odot h^{-1})$)	C_{cen}	M_1 ($M_\odot h^{-1}$)	M_{cut} ($M_\odot h^{-1}$)	α_{HOD}	No. of Galaxies
−21.5	12.83 ± 0.03	1.53 ± 0.07	0.239 ± 0.011	14.33 ± 0.02	12.2 ± 0.6	1.06 ± 0.07	4437
−21.0	12.49 ± 0.01	1.26 ± 0.02	0.497 ± 0.007	13.72 ± 0.01	12.51 ± 0.08	0.948 ± 0.023	16062
−20.5	12.217 ± 0.003	1.108 ± 0.008	0.784 ± 0.003	13.27 ± 0.01	12.37 ± 0.04	0.948 ± 0.013	49718
−20.0	11.936 ± 0.002	0.959 ± 0.005	0.936 ± 0.002	12.954 ± 0.007	12.16 ± 0.02	0.949 ± 0.008	103906
−19.5	11.701 ± 0.001	0.812 ± 0.003	0.9854 ± 0.0005	12.736 ± 0.005	11.97 ± 0.02	0.960 ± 0.005	174937
−19.0	11.503 ± 0.001	0.723 ± 0.002	0.9975 ± 0.0002	12.567 ± 0.004	11.81 ± 0.01	0.966 ± 0.004	261921

Table 8
Luminosity HOD Parameters for Zehavi Fit

M_r Threshold	$\log M_{\text{min}}$ ($\log(M_\odot h^{-1})$)	$\sigma_{\log M}$ ($\log(M_\odot h^{-1})$)	$\log M_0$ ($\log(M_\odot h^{-1})$)	$\log M'_1$ ($\log(M_\odot h^{-1})$)	α_{HOD}	No. of Galaxies
−21.5	13.75 ± 0.03	1.13 ± 0.03	13.75 ± 0.38	14.35 ± 0.12	1.33 ± 0.47	4437
−21.0	12.83 ± 0.01	0.731 ± 0.009	13.26 ± 0.07	13.80 ± 0.03	1.06 ± 0.06	18062
−20.5	12.293 ± 0.003	0.514 ± 0.004	12.73 ± 0.02	13.29 ± 0.01	0.965 ± 0.014	49715
−20.0	11.919 ± 0.002	0.392 ± 0.003	12.31 ± 0.01	12.947 ± 0.005	0.945 ± 0.007	103904
−19.5	11.682 ± 0.001	0.321 ± 0.002	11.682 ± 0.007	12.729 ± 0.004	0.953 ± 0.004	174932
−19.0	11.491 ± 0.001	0.295 ± 0.001	11.491 ± 0.008	12.580 ± 0.003	0.977 ± 0.003	261915

APPENDIX D

LUMINOSITY HOD COMPARISON TO SDSS

To perform a more exact comparison with the HOD of Zehavi et al. (2011), we use the best-fit luminosity-based abundance matching model. This model has parameters $\mu_{\text{cut}} = 0.13$ and scatter of 0.22 dex, and well reproduces the SDSS clustering of Zehavi et al. (2011), as shown in Appendix C. We measure the HOD directly from the model, then perform a fit to the total HOD using the fitting function of Zehavi et al. (2011):

$$\langle N \rangle = \frac{1}{2} \left[1 + \operatorname{erf} \left(\frac{\log M_h - \log M_{\text{min}}}{\sigma_{\log M}} \right) \right] \cdot \left[1 + \left(\frac{M_h - M_0}{M'_1} \right)^{\alpha_{\text{HOD}}} \right]. \quad (\text{D1})$$

The final term gives the central and satellite parts, with the power-law-like satellite part being set to zero when $M_h < M_0$.

The results of this fit, along with comparison to the results of Zehavi et al. (2011) and our parameterization of the HOD, are shown in Figure 27. The parameters for the luminosity model using this fitting function are given in Table 8. Both this figure and a comparison of the parameters indicate nearly the same behavior as described for the HODs in the stellar mass model. Our model implies a higher and broader central mass cutoff then seen in Zehavi et al. (2011). The fit for the satellite part is generally consistent between the two cases. However, due to the high μ_{cut} and scatter, the central part of the HOD

never reaches unity for the brightest luminosity thresholds. While the overall HOD can be well fit with Equation (D1), the centrals and satellites separately are not, particularly at the brighter thresholds. This serves as additional motivation for our explicit separation of the central and satellite parts of the HOD. For the luminosity case, we multiply Equation (9) by an additional overall normalization parameter to account for the reduced maximum number of central galaxies. The closeness of the fits in general makes it difficult to claim a significant difference between the Zehavi et al. (2011) results and our fits. Further, in the highest luminosity thresholds where the differences are largest, the clustering produced by our model is also somewhat low. This is in agreement with the shift of the brightest luminosity HOD to somewhat lower host halo masses, and thus, lower bias, which also obscures the comparison.

APPENDIX E

RADIAL PROFILES

Projected radial profiles are presented, as a further test of the input catalog and the group-finding algorithm. These show the satellites assigned to groups for each host halo mass, and give their projected number density at distances from the group center. The group center is determined by the location of the central, and distances are given as a fraction of the virial radius. Figure 28 shows the profiles in the stellar mass best-fit case for two different cuts in stellar mass, and the same result for one cut in the best-fit luminosity model.

The larger differences in the profiles in the luminosity case may help explain why the luminosity model fits more poorly overall. The higher μ_{cut} preferentially removes satellites near the centers of clusters which have already been significantly stripped. This impacts the CSMF, but the change in radial profile shape also impacts the one-halo term in the clustering. Further discussion of satellite incompleteness and its dependence on galaxy luminosity and simulation specifications will be given in Wu et al. (2013).

REFERENCES

- Abazajian, K. N., Adelman-McCarthy, J. K., Agüeros, M. A., et al. 2009, *ApJS*, **182**, 543
- Baldry, I. K., Driver, S. P., Loveday, J., et al. 2012, *MNRAS*, **421**, 621
- Behroozi, P. S., Conroy, C., & Wechsler, R. H. 2010, *ApJ*, **717**, 379
- Behroozi, P. S., Wechsler, R. H., & Conroy, C. 2013a, *ApJ*, **770**, 57
- Behroozi, P. S., Wechsler, R. H., & Wu, H.-Y. 2013b, *ApJ*, **762**, 109
- Behroozi, P. S., Wechsler, R. H., Wu, H.-Y., et al. 2013c, *ApJ*, **763**, 18
- Bell, E. F., McIntosh, D. H., Katz, N., & Weinberg, M. D. 2003, *ApJS*, **149**, 289
- Benson, A. J. 2012, *NewA*, **17**, 175
- Blanton, M. R., Hogg, D. W., Bahcall, N. A., et al. 2003a, *ApJ*, **592**, 819
- Blanton, M. R., Lin, H., Lupton, R. H., et al. 2003b, *AJ*, **125**, 2276
- Blanton, M. R., & Roweis, S. 2007, *AJ*, **133**, 734
- Blanton, M. R., Schlegel, D. J., Strauss, M. A., et al. 2005, *AJ*, **129**, 2562
- Bryan, G. L., & Norman, M. L. 1998, *ApJ*, **495**, 80
- Cacciato, M., van den Bosch, F. C., More, S., et al. 2009, *MNRAS*, **394**, 929
- Chabrier, G. 2003, *PASP*, **115**, 763
- Conroy, C., Wechsler, R. H., & Kravtsov, A. V. 2006, *ApJ*, **647**, 201
- Davis, M., Efstathiou, G., Frenk, C. S., & White, S. D. M. 1985, *ApJ*, **292**, 371
- Gao, L., & White, S. D. M. 2007, *MNRAS*, **377**, L5
- George, M. R., Leauthaud, A., Bundy, K., et al. 2012, *ApJ*, **757**, 2
- Guo, Q., White, S., Boylan-Kolchin, M., et al. 2011, *MNRAS*, **413**, 101
- Hansen, S. M., Sheldon, E. S., Wechsler, R. H., & Koester, B. P. 2009, *ApJ*, **699**, 1333
- Hearin, A. P., Zentner, A. R., Newman, J. A., & Berlind, A. A. 2013, *MNRAS*, **430**, 1238
- Henriques, B. M. B., White, S. D. M., Lemson, G., et al. 2012, *MNRAS*, **421**, 2904
- Klypin, A., Gottlöber, S., Kravtsov, A. V., & Khokhlov, A. M. 1999, *ApJ*, **516**, 530
- Klypin, A. A., Trujillo-Gomez, S., & Primack, J. 2011, *ApJ*, **740**, 102
- Knebe, A., Knollmann, S. R., Muldrew, S. I., et al. 2011, *MNRAS*, **415**, 2293
- Koester, B. P., McKay, T. A., Annis, J., et al. 2007, *ApJ*, **660**, 239
- Kravtsov, A. V., Berlind, A. A., Wechsler, R. H., et al. 2004, *ApJ*, **609**, 35
- Kroupa, P. 2001, *MNRAS*, **322**, 231
- Landy, S. D., & Szalay, A. S. 1993, *ApJ*, **412**, 64
- Leauthaud, A., Tinker, J., Behroozi, P. S., Busha, M. T., & Wechsler, R. H. 2011, *ApJ*, **738**, 45
- Leauthaud, A., Tinker, J., Bundy, K., et al. 2012, *ApJ*, **744**, 159
- Li, C., & White, S. D. M. 2009, *MNRAS*, **398**, 2177
- Lu, Y., Mo, H. J., Katz, N., & Weinberg, M. D. 2012, *MNRAS*, **421**, 1779
- McBride, C., Berlind, A., Scoccimarro, R., et al. 2009, *BAAS*, **41**, 253
- Mocz, P., Green, A., Malacari, M., & Glazebrook, K. 2012, *MNRAS*, **425**, 296
- More, S., van den Bosch, F., Cacciato, M., et al. 2012, arXiv:1204.0786
- More, S., van den Bosch, F. C., Cacciato, M., et al. 2009, *MNRAS*, **392**, 801
- Moster, B. P., Somerville, R. S., Maulbetsch, C., et al. 2010, *ApJ*, **710**, 903
- Moustakas, J., Coil, A., Aird, J., et al. 2013, *ApJ*, **767**, 50
- Neistein, E., Li, C., Khochfar, S., et al. 2011a, *MNRAS*, **416**, 1486
- Neistein, E., Weinmann, S. M., Li, C., & Boylan-Kolchin, M. 2011b, *MNRAS*, **414**, 1405
- Nuza, S. E., Sanchez, A. G., Prada, F., et al. 2013, *MNRAS*, **432**, 743
- Onions, J., Knebe, A., Pearce, F. R., et al. 2012, *MNRAS*, **423**, 1200
- Padmanabhan, N., Schlegel, D. J., Finkbeiner, D. P., et al. 2008, *ApJ*, **674**, 1217
- Rodríguez-Puebla, A., Drory, N., & Avila-Reese, V. 2012, *ApJ*, **756**, 2
- Rozo, E., Wechsler, R. H., Rykoff, E. S., et al. 2010, *ApJ*, **708**, 645
- Simha, V., Weinberg, D. H., Davé, R., et al. 2012, *MNRAS*, **423**, 3458
- Skibba, R. A., van den Bosch, F. C., Yang, X., et al. 2011, *MNRAS*, **410**, 417
- Somerville, R. S., Gilmore, R. C., Primack, J. R., & Domínguez, A. 2012, *MNRAS*, **423**, 1992
- Springel, V., & Hernquist, L. 2003, *MNRAS*, **339**, 289
- Springel, V., White, S. D. M., Jenkins, A., et al. 2005, *Natur*, **435**, 629
- Stoughton, C., Lupton, R. H., Bernardi, M., et al. 2002, *AJ*, **123**, 485
- Suyu, S. H., Marshall, P. J., Auger, M. W., et al. 2010, *ApJ*, **711**, 201
- Tasitsiomi, A., Kravtsov, A. V., Wechsler, R. H., & Primack, J. R. 2004, *ApJ*, **614**, 533
- Tinker, J., Kravtsov, A. V., Klypin, A., et al. 2008, *ApJ*, **688**, 709
- Tinker, J., Wetzel, A., & Conroy, C. 2011, arXiv:1107.5046
- Tinker, J. L., Sheldon, E. S., Wechsler, R. H., et al. 2012, *ApJ*, **745**, 16
- Trujillo-Gomez, S., Klypin, A., Primack, J., & Romanowsky, A. J. 2011, *ApJ*, **742**, 16
- Vale, A., & Ostriker, J. P. 2004, *MNRAS*, **353**, 189
- Vale, A., & Ostriker, J. P. 2006, *MNRAS*, **371**, 1173
- Vogelsberger, M., Sijacki, D., Kereš, D., Springel, V., & Hernquist, L. 2012, *MNRAS*, **425**, 3024
- Watson, D. F., Berlind, A. A., & Zentner, A. R. 2011, *ApJ*, **738**, 22
- Watson, D. F., Berlind, A. A., & Zentner, A. R. 2012, *ApJ*, **754**, 90
- Wechsler, R. H. 2001, PhD thesis, Univ. California, Santa Cruz
- Wechsler, R. H., Zentner, A. R., Bullock, J. S., Kravtsov, A. V., & Allgood, B. 2006, *ApJ*, **652**, 71
- Wetzel, A. R., & White, M. 2010, *MNRAS*, **403**, 1072
- Wu, H.-Y., Hahn, O., Wechsler, R. H., Behroozi, P. S., & Mao, Y.-Y. 2013, *ApJ*, **767**, 23
- Yang, X., Mo, H. J., & van den Bosch, F. C. 2003, *MNRAS*, **339**, 1057
- Yang, X., Mo, H. J., & van den Bosch, F. C. 2008, *ApJ*, **676**, 248
- Yang, X., Mo, H. J., & van den Bosch, F. C. 2009, *ApJ*, **695**, 900
- Yang, X., Mo, H. J., van den Bosch, F. C., & Jing, Y. P. 2005, *MNRAS*, **356**, 1293
- Yang, X., Mo, H. J., van den Bosch, F. C., Zhang, Y., & Han, J. 2012, *ApJ*, **752**, 41
- Yang, X., Mo, H. J., van den Bosch, F. C., et al. 2007, *ApJ*, **671**, 153
- Zehavi, I., Zheng, Z., Weinberg, D. H., et al. 2005, *ApJ*, **630**, 1
- Zehavi, I., Zheng, Z., Weinberg, D. H., et al. 2011, *ApJ*, **736**, 59
- Zentner, A. R., Berlind, A. A., Bullock, J. S., Kravtsov, A. V., & Wechsler, R. H. 2005, *ApJ*, **624**, 505
- Zheng, Z., Coil, A. L., & Zehavi, I. 2007, *ApJ*, **667**, 760